

Electronic Supplementary Information

Effects of organic ligands, phosphate and Ca on the structure and composition of Fe(III)-precipitates formed by Fe(II) oxidation at near-neutral pH

Ville V. Nenonen^{a,b}, Ralf Kaegi^a, Stephan J. Hug^a, Jörg Luster^c, Jörg Göttlicher^d,
Stefan Mangold^d, Lenny H.E. Winkel^{a,b}, Andreas Voegelin^{a,*}

^a Eawag, Swiss Federal Institute of Aquatic Science and Technology, Überlandstrasse 133, CH-8600 Dübendorf, Switzerland

^b ETH Zurich, Swiss Federal Institute of Technology, Institute of Biogeochemistry and Pollutant Dynamics, Universitätstrasse 16, CH-8092 Zürich, Switzerland

^c WSL, Swiss Federal Institute for Forest, Snow and Landscape Research, Zürcherstrasse 111, CH-8903 Birmensdorf, Switzerland

^d Karlsruhe Institute of Technology, Institute for Photon Science and Synchrotron radiation, Hermann-von-Helmholtz Platz 1, D-76344 Eggenstein-Leopoldshafen, Germany

* Correspondence: andreas.voegelin@eawag.ch

Contents

1	Structure of organic ligands and thermodynamic calculations.....	3
2	Experimental treatments and analytical methods	7
3	Elemental composition of Fe(III)-precipitates	8
4	X-ray absorption spectroscopy	9
5	X-ray diffraction.....	16
6	Fourier-transform infrared spectroscopy (FTIR).....	18
7	Scanning transmission electron microscopy	19
8	Dynamic light scattering	30
9	Turbidity.....	33
10	TOC analyses in solution	40
11	UV-Vis	41
12	Ligand/Fe ratios of selected precipitates and of LCF-based precipitate fractions.....	43
13	References	44

1 Structure of organic ligands and thermodynamic calculations

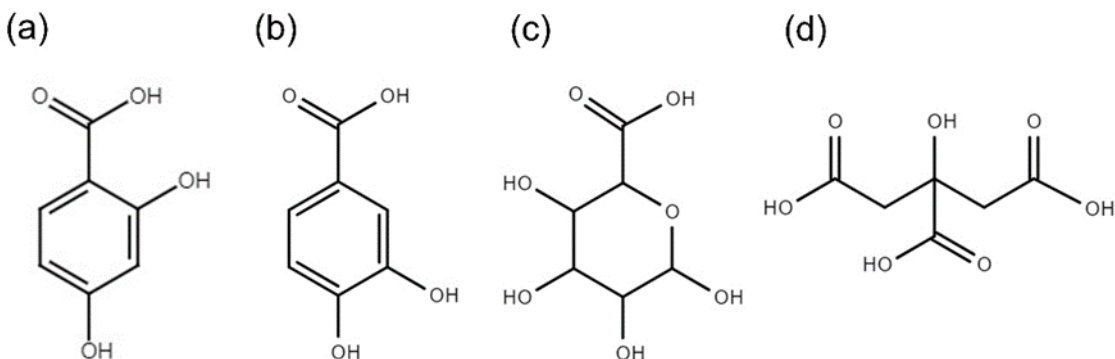


Figure S1. Structures of model ligands used in this study. (a) 2,4-dihydroxybenzoic acid (2,4-DHB) (b) 3,4-dihydroxybenzoic acid (3,4-DHB) (c) galacturonic acid (Galact) (d) citric acid (Citr).

Deprotonation and complex stability constants

The structures of the four low molecular weight organic acid (LMWOA) used as model ligands in this study are shown in Fig. S1. Owing to their different structures, they form different types of complexes with Fe³⁺ with different stoichiometries. To compare the extent of Fe(III) complexation by the four ligands, thermodynamic equilibrium calculations were conducted with PHREEQC using the MINTEQA4 equilibrium constants database.¹ Additional equilibrium constants for the deprotonation and Fe(III) and Ca complexation of the four organic ligands (where available) were taken from the NIST Standard Reference Database 46 v. 8.0 (Critically Selected Stability Constants of Metal Complexes)² and, for galacturonic acid, from Deiana et al. (1989).³ The reported constants (for defined ionic strengths) were recalculated to zero ionic strength, using the Davies equation to calculate the activity coefficients of charged reactants and without activity correction for uncharged molecules. The deprotonation and complex formation constants are listed in Table S1.

Thermodynamic calculations

The calculations were performed starting from solutions containing 8 mM NaHCO₃ or 4 mM CaCO₃, 0.5 mM Fe(III)(NO₃)₃ (equivalent to complete Fe(II) oxidation; NO₃⁻ as weakly complexing counter anion), and the individual organic ligand at a concentration equivalent to molar (OC/Fe)_{init} ratios of 0.6 (0.05 mM of Citr or Galact; 0.043 mM of 24-DHB or 34-DHB) or 9.6 (0.8 mM Citr, 0.69 mM 3,4-DHB). In the equilibration step, ferrihydrite was allowed to precipitate and the pH was buffered to pH 7.0 using the bicarbonate buffer system, i.e., by adjusting the CO₂ partial pressure. In all calculations, the sum of all inorganic Fe species equals ~4.8×10⁻⁹ M (mainly Fe(OH)₂⁺ and Fe(OH)₃ complexes), in equilibrium with ferrihydrite at pH 7.0.

Na electrolytes at (OC/Fe)_{init} 0.6. In the Na electrolyte at (OC/Fe)_{init} 0.6, most extensive Fe(III) complexation results for Citr, followed by 3,4-DHB. In the case of Citr, the concentration of organically-

complexed Fe(III) exceeds the concentration of inorganic Fe(III) by 3 orders of magnitude, and about 10% of the total Citr in solution is complexed with Fe. Yet, even in the case of Citr at $(OC/Fe)_{init}$ 0.6, only a minor fraction of 1.0% of the total Fe(III) (0.5 mM) remains in solution, and most Fe(III) forms ferrihydrite. In the case of 3,4-DHB, organically complexed Fe(III) still exceeds inorganic Fe(III) in solution by factor ~5. For Galact and 2,4-DHB, the calculations indicate only minor Fe(III)-ligand complexation, and total dissolved Fe(III) is dominated by inorganic Fe(III). The calculations suggest about 5-fold weaker Fe(III) complexation by Galact than 2,4-DHB.

Ca electrolytes at $(OC/Fe)_{init}$ 0.6 (Citr, 3,4-DHB). In Ca electrolytes, the complexation of the organic ligands with Ca may influence their interactions with Fe(III). For Citr and 3,4-DHB, speciation calculations for 4 mM Ca electrolyte at $(OC/Fe)_{init}$ 0.6 showed that about 98% of the total Citr is present as $Ca(Citrate)^-$ complex, thereby reducing the effect of citrate on Fe(III), as reflected in an about 80 times lower concentration of Citr-complexed dissolved Fe(III). Owing to the weak complexation of Ca by 3,4-DHB, on the other hand, only minor differences in Fe(III) complexation by 3,4-DHB occur between the Na and Ca electrolytes. Therefore, direct effects of Ca on Fe(III) complexation were only expected for Citr.

Citr and 3,4-DHB at $(OC/Fe)_{init}$ 9.6. Calculations for Citr and 3,4-DHB were also carried out for $(OC/Fe)_{init}$ 9.6, corresponding to molar ligand/Fe(III) ratios of 1.6 Citr/Fe or 1.4 3,4-DHB; i.e., an excess of the organic ligands over total Fe(III). The results indicated that in Na electrolyte, Citr could retain a significant fraction of the total Fe (44%) in solution via complex formation, whereas 3,4-DHB would still only complex a minor share of the total Fe(III). In the Ca electrolyte, however, Ca complexation with Citr is predicted to reduce its effect on Fe(III) to a level comparable to 3,4-DHB.

Citr and 3,4-DHB: L/Fe ratios. According to the model calculations, the $Fe(OH)L^-$ complex was the dominant complex of Citr at $(OC/Fe)_{init}$ 0.6 in both Na and Ca electrolyte and at $(OC/Fe)_{init}$ 9.6 in Ca electrolyte, whereas at $(OC/Fe)_{init}$ 9.6 in Na electrolyte, the $Fe_2(OH)_2L_2^{2-}$ complex dominated. In both cases, however, the L/Fe ratio equals unity. For 3,4-DHB, on the other hand, the $Fe(OH)L^-$ complex dominated at $(OC/Fe)_{init}$ 0.6 and the FeL_2^{-3} complex at $(OC/Fe)_{init}$ 9.6, in both the Na and Ca electrolyte, corresponding to a shift in the L/Fe ratio from 1 to 2.

Table S1. Equilibrium constants for the deprotonation and Fe(III) and Ca complexation of the studied low molecular weight organic acids.

Reaction	Log K	Source
citric acid = H₃L		
H ₃ L = H ₂ L ⁻ + H ⁺	-3.128	MINTEQA2 V4
H ₂ L ⁻ = HL ²⁻ + H ⁺	-4.761	MINTEQA2 V4
HL ²⁻ = L ³⁻ + H ⁺	-6.396	MINTEQA2 V4
Fe ³⁺ + L ³⁻ = FeL	13.1	MINTEQA2 V4
Fe ³⁺ + L ³⁻ + H ⁺ = Fe(HL)	14.4	MINTEQA2 V4
FeL + H ₂ O = Fe(OH)L ⁻ + H ⁺	-3.0	NIST 46
2Fe ³⁺ + 2L ³⁻ + 2H ₂ O = Fe ₂ (OH) ₂ L ₂ ²⁻ + 2H ⁺	24.9	NIST 46
Ca ²⁺ + L ³⁻ = CaL ⁻	4.87	MINTEQA2 V4
Ca ²⁺ + L ³⁻ + H ⁺ = Ca(HL)	9.26	MINTEQA2 V4
Ca ²⁺ + L ³⁻ + 2H ⁺ = Ca(H ₂ L) ⁺	12.257	MINTEQA2 V4
3,4-dihydroxybenzoic acid = H₃L		
H ₃ L = H ₂ L ⁻ + H ⁺	-4.60	NIST 46
H ₂ L ⁻ = HL ²⁻ + H ⁺	-9.27	NIST 46
HL ²⁻ = L ³⁻ + H ⁺	-13.76	NIST 46
H ₂ L ⁻ + Fe ³⁺ = FeL + 2H ⁺	-1.35	NIST 46
H ₂ L ⁻ + FeL = FeL ₂ ³⁻ + 2H ⁺	-8.79	NIST 46
H ₂ L ⁻ + FeL ₂ ³⁻ = FeL ₃ ⁶⁻ + 2H ⁺	-16.58	NIST 46
FeL + H ⁺ = Fe(HL) ⁺	4.70	NIST 46
Fe(HL) ⁺ + H ⁺ = Fe(H ₂ L) ²⁺	1.89	NIST 46
FeL + H ₂ O = Fe(OH)L ⁻ + H ⁺	-5.16	NIST 46
Fe(OH)L ⁻ + H ₂ O = Fe(OH) ₂ L ²⁻ + H ⁺	-8.62	NIST 46
H ₂ L ⁻ + Ca ²⁺ = CaL ⁻ + 2H ⁺	-16.69	NIST 46
H ₂ L ⁻ + CaL ⁻ = CaL ₂ ⁴⁻ + 2H ⁺	-19.94	NIST 46
galacturonic acid = H₃L		
H ₃ L = H ₂ L ⁻ + H ⁺	-3.51	NIST 46
H ₂ L ⁻ = HL ²⁻ + H ⁺	na	
HL ²⁻ = L ³⁻ + H ⁺	na	
H ₂ L ⁻ + Fe ³⁺ = Fe(HL) ⁺ + H ⁺	2.05	NIST 46
Fe(HL) ⁺ = FeL + H ⁺	-4.48	NIST 46
3H ₂ L ⁻ + Fe ³⁺ = Fe(H ₂ L) ₃	12.76	Deiana et al. (1989)
3H ₂ L ⁻ + Fe ³⁺ = Fe(HL) ₂ (H ₂ L) ²⁻ + 2H ⁺	3.37	Deiana et al. (1989)
3H ₂ L ⁻ + Fe ³⁺ = Fe(HL) ₃ ³⁻ + 3H ⁺	-2.03	Deiana et al. (1989)
H ₂ L ⁻ + Ca ²⁺ = Ca(HL) + H ⁺	-8.83	NIST 46
2,4-dihydroxybenzoic acid = H₃L		
H ₃ L = H ₂ L ⁻ + H ⁺	-3.43	NIST 46
H ₂ L ⁻ = HL ²⁻ + H ⁺	-9.16	NIST 46
HL ²⁻ = L ³⁻ + H ⁺	na	
H ₂ L ⁻ + Fe ³⁺ = Fe(HL) ⁺ + H ⁺	4.12	NIST 46
H ₂ L ⁻ + Fe(HL) ⁺ = Fe(HL) ₂ ²⁻ + H ⁺	-1.39	NIST 46
H ₂ L ⁻ + Fe(HL) ₂ ²⁻ = Fe(HL) ₃ ³⁻ + H ⁺	-6.38	NIST 46
H ₂ L ⁻ + Fe ³⁺ = Fe(H ₂ L) ²⁺	5.91	NIST 46

Table S2. Thermodynamic calculations of Fe(III) speciation in suspensions with 0.5 mM total Fe(III) in equilibrium with ferrihydrite. Calculations performed for organic ligands at $(OC/Fe)_{init}$ of 0.6 and 9.6 in Na or Ca electrolyte at pH 7.0 (buffered by bicarbonate/CO₂).

Ligand	Cation	$(OC/Fe)_{init}$	dissolved Fe				dissolved L bound to Fe (%total)
			total (mol/L)	(%initial)	inorganic (mol/L)	organic (mol/L)	
control	Na	0.0	4.8E-09	0.0010%	4.8E-09	na	na
2,4-DHB	Na	0.6	4.9E-09	0.0010%	4.8E-09	1.5E-10	0.00066%
Galact	Na	0.6	4.8E-09	0.0010%	4.8E-09	2.9E-11	0.000072%
3,4-DHB	Na	0.6	3.0E-08	0.0060%	4.8E-09	2.5E-08	0.068%
Citr	Na	0.6	4.8E-06	1.0%	4.8E-09	4.8E-06	10%
3,4-DHB	Ca	0.6	3.1E-08	0.0061%	4.8E-09	2.6E-08	0.070%
Citr	Ca	0.6	5.9E-08	0.012%	4.8E-09	5.4E-08	0.11%
3,4-DHB	Na	9.6	1.4E-06	0.28%	4.8E-09	1.4E-06	0.36%
Citr	Na	9.6	2.2E-04	44.1%	4.8E-09	2.2E-04	28%
3,4-DHB	Ca	9.6	1.5E-06	0.30%	4.9E-09	1.5E-06	0.39%
Citr	Ca	9.6	1.2E-06	0.24%	4.8E-09	1.2E-06	0.15%

2 Experimental treatments and analytical methods

Table S3. Overview over experiments and treatments (cations, (P/Fe)_{init}, ligands and (OC/Fe)_{init} ratios).

Experiment	Electrolyte	Volume (mL)	(P/Fe) _{init}	Ligand and (OC/Fe) _{init}				
				LH	2,4-DHB	Galact	3,4-DHB	Citr
E05	Ca, Na	200	0.05, 0.25	0.6, 2.4	0.6, 2.4	0.6, 2.4	-	0.6, 2.4
E07	Ca, Na	200	0.05	0.3, 0.6, 1.2, 2.4, 9.6	0.3, 0.6, 1.2, 2.4, 9.6	0.3, 0.6, 1.2, 2.4, 9.6	-	0.3
E13	Ca, Na	600	0.05, 0.25	0.6, 2.4, 9.6	0.6, 2.4, 9.6	0.6, 2.4, 9.6	-	0.1, 0.3, 0.6
E15	Ca, Na	600	0.05, 0.25	0.6, 2.4, 9.6	0.6, 2.4, 9.6	0.6, 2.4, 9.6	0.6, 2.4, 9.6	0.1, 0.3, 0.6, 1.2
E20	Na	600	0.05, 0.25	-	-	-	0.1, 0.3, 0.6	-
E22	Ca, Na	200	0.05, 0.25	-	-	-	0.6, 1.2, 2.4, 9.6	0.6, 1.2, 2.4, 9.6

Table S4. Overview over analytical techniques used in different experiments.

Experiment	Solids				Suspensions				Solution		
	XAS	XRD + FTIR	Acid digest	soliTOC	STEM	DLS	ELS	Turbidity	ICP- MS	DOC	UV- vis
E05	-	-	-	-	-	X	-	-	X	-	-
E07	-	-	-	-	-	X	X	-	X	X	-
E13	X	X	X	X	X	X	X	-	X	X	-
E15	X	X	X	X	X	X	X	X	X	X	X
E20	-	X	X	X	X	X	X	X	X	X	-
E22	-	-	-	-	-	X	X	-	X	X	-

3 Elemental composition of Fe(III)-precipitates

Table S5. Molar ratios $(P/Fe)_{ppt}$, $(Ca/Fe)_{ppt}$, and $(OC/Fe)_{ppt}$ of precipitates formed at $(P/Fe)_{init}$ 0.05 and 0.25 in Ca and Na electrolytes. Ratios were derived from contents of Fe, P, and Ca determined by acid digestion (duplicate analysis of single digests) and of OC contents from dry combustion (single samples). First two columns indicate experiments from which samples for analysis by acid digestion or dry combustion (OC) were derived.

Exp Digest	Exp OC	Ligand	$(OC/Fe)_{init}$	$(P/Fe)_{init}$ 0.05				
				Ca			Na	
				$(P/Fe)_{ppt}$	$(Ca/Fe)_{ppt}$	$(OC/Fe)_{ppt}$	$(P/Fe)_{ppt}$	$(OC/Fe)_{ppt}$
E15	E15	Ctrl	0	0.042	0.060	0.00	0.031	0.00
E13	E15	2,4-DHB	0.6	0.046	0.055	0.04	0.036	0.04
E13	E15	2,4-DHB	2.4	0.048	0.061	0.10	0.040	0.07
E13	E15	2,4-DHB	9.6	0.050	0.085	0.35	0.045	0.23
E13	E15	Galact	0.6	0.047	0.059	0.05	0.044	0.06
E13	E15	Galact	2.4	0.052	0.104	0.15	0.057	0.12
E13	E15	Galact	9.6	0.052	0.102	0.46	0.058	0.33
E15	E15	3,4-DHB	0.6	0.049	0.095	0.57	0.042	0.47
E15	E15	3,4-DHB	2.4	0.051	0.162	1.29	NS ^a	NS ^a
E15	E15	3,4-DHB	9.6	0.087	0.203	2.65	NS ^a	NS ^a
E13	E15	Citr	0.1	0.046	0.074	0.07	0.043	0.09
E13	E15	Citr	0.3	0.049	0.120	0.24	NS ^a	NS ^a
E13	E15	Citr	0.6	0.050	0.136	0.46	NS ^a	NS ^a
E13	E13	LH	0.6	0.046	0.070	0.52	# ^b	# ^b
E13	E13	LH	2.4	0.045	0.156	1.73	0.045	3.14
E13	E13	LH	9.6	0.044	0.425	8.23	0.044	2.63
				$(P/Fe)_{init}$ 0.25				
E15	E15	Ctrl	0	0.224	0.148	0.00	0.189	0.00
E13	E15	2,4-DHB	0.6	0.234	0.151	0.04	0.197	0.03
E13	E15	2,4-DHB	2.4	0.234	0.190	0.08	0.205	0.05
E13	E15	2,4-DHB	9.6	0.239	0.155	0.23	0.212	0.12
E13	E15	Galact	0.6	0.245	0.188	0.06	0.206	0.03
E13	E15	Galact	2.4	0.247	0.178	0.13	0.235	0.08
E13	E15	Galact	9.6	0.236	0.153	0.45	0.238	0.25
E15	E15	3,4-DHB	0.6	0.241	0.199	0.44	0.232	0.35
E15	E15	3,4-DHB	2.4	0.259	0.243	1.17	NS ^a	NS ^a
E15	E15	3,4-DHB	9.6	0.497	0.406	1.88	NS ^a	NS ^a
E13	E15	Citr	0.1	0.233	0.170	0.06	0.211	0.07
E13	E15	Citr	0.3	0.238	0.215	0.21	NS ^a	NS ^a
E13	E15	Citr	0.6	0.240	0.262	0.36	NS ^a	NS ^a
E13	E13	LH	0.6	0.232	0.186	0.52	# ^b	# ^b
E13	E13	LH	2.4	0.222	0.245	1.64	0.148	2.91
E13	E13	LH	9.6	0.227	0.457	7.59	0.167	8.34

^a solids attached strongly on the membrane and could not be removed (#)

^b solids passed through the membrane, no filter recoverable solids (NS)

4 X-ray absorption spectroscopy

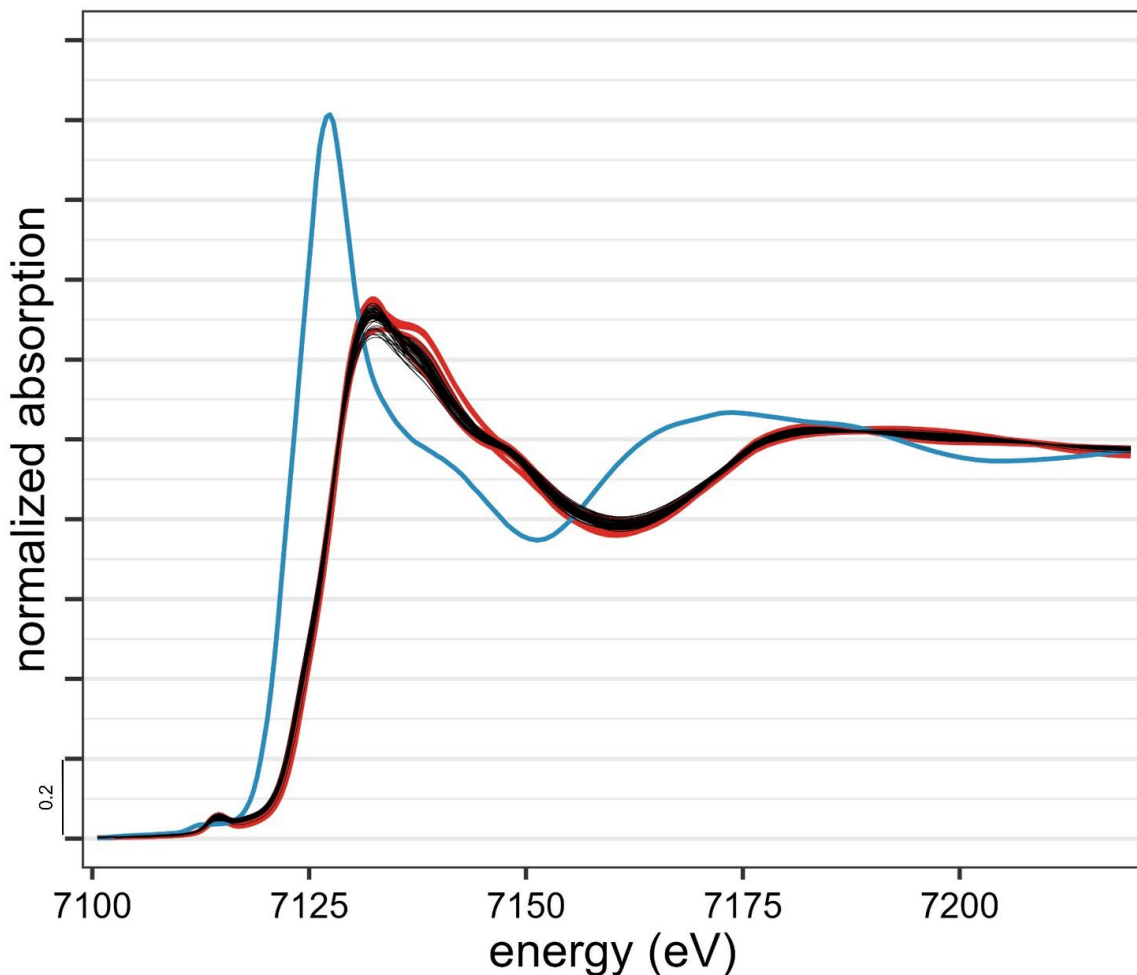


Figure S2. Normalized Fe K-edge XANES spectra of all sample spectra (thin black lines), all Fe(III)-precipitate reference spectra used for LCF analysis (red lines), and a reference spectrum of dissolved Fe^{2+} (50 mM FeSO_4 , 1 mM HCl; blue line).

The comparison of the sample and Fe(III)-precipitate reference spectra used for EXAFS LCF analysis with the spectrum of aqueous Fe(II) points to negligible fractions of Fe(II) in the sample spectra.

In line with this qualitative assessment, LCF analysis of the sample EXAFS spectra using the reference spectrum of dissolved Fe^{2+} as 6th spectral component returned a negligible fraction of Fe(II) (average fitted Fe^{2+} fraction: 0.006; 90-percentile fraction: 0.015; highest fitted fraction: 0.035; n = 61 spectra).

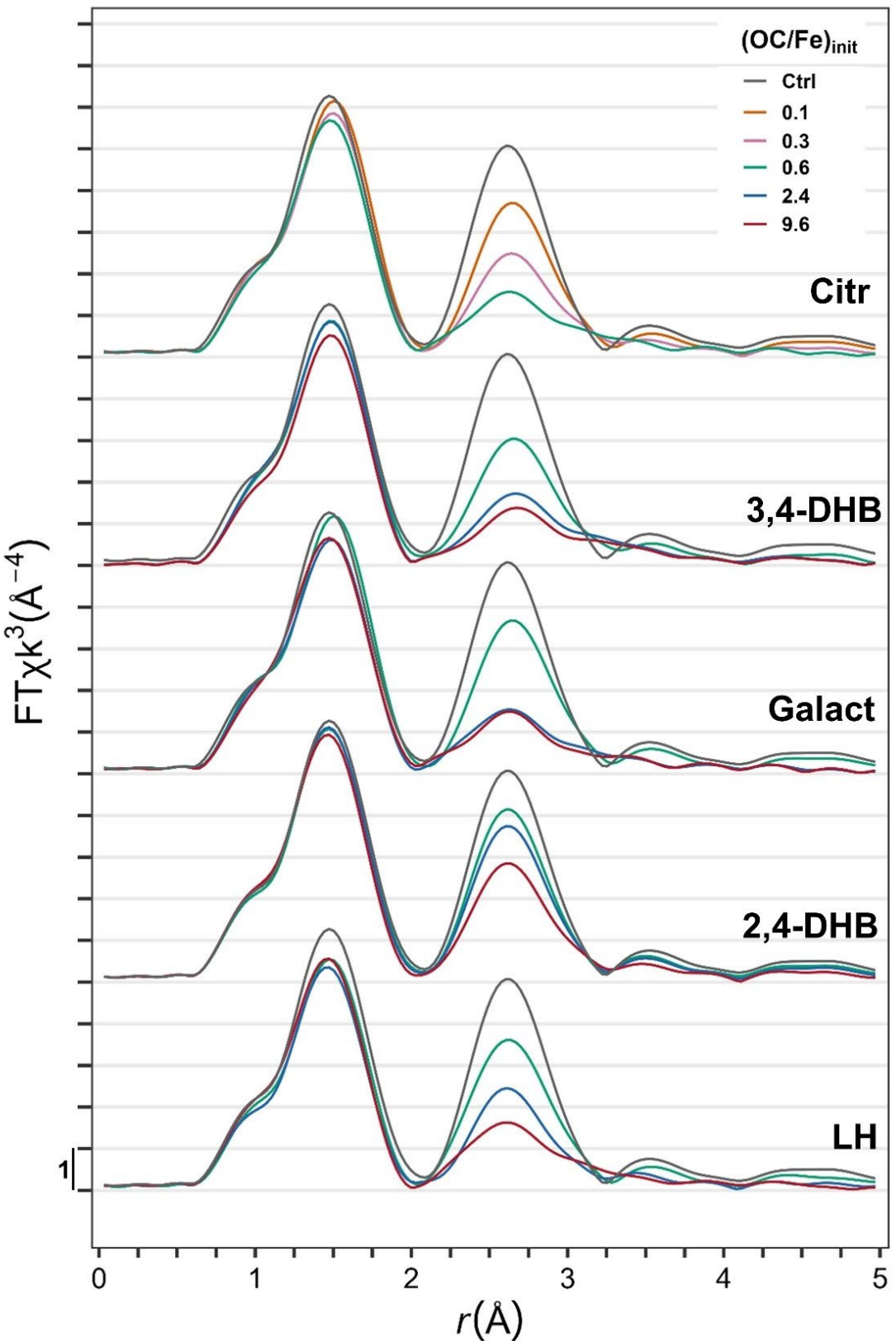


Figure S3. Fourier-transformed EXAFS spectra of precipitates formed at Ca 0.25.

Table S6. LCF results for precipitates formed at $(\text{P}/\text{Fe})_{\text{init}}$ 0.05

Experiment	Electrolyte	Organic	$(\text{OC}/\text{Fe})_{\text{init}}$	Lp*	Fh*	FeP*	CaFeP*	FeOrg*	r-factor
E13	Ca	Ctrl	0.0	0.83	0.11	0.04	0.00	0.00	0.00371
E15	Ca	Ctrl	0.0	0.80	0.17	0.02	0.00	0.00	0.000612
E13	Ca	2,4-DHB	0.6	0.76	0.13	0.04	0.00	0.00	0.000352
E13	Ca	2,4-DHB	2.4	0.62	0.34	0.00	0.00	0.01	0.000313
E13	Ca	2,4-DHB	9.6	0.28	0.69	0.00	0.00	0.02	0.000479
E13	Ca	Galact	0.6	0.66	0.32	0.01	0.00	0.00	0.000451
E13	Ca	Galact	2.4	0.01	0.91	0.00	0.01	0.06	0.000715
E13	Ca	Galact	9.6	0.00	0.80	0.10	0.00	0.09	0.001274
E15	Ca	3,4-DHB	0.6	0.12	0.66	0.00	0.03	0.16	0.000979
E15	Ca	3,4-DHB	2.4	0.07	0.70	0.00	0.00	0.22	0.002089
E15	Ca	3,4-DHB	9.6	0.05	0.54	0.00	0.00	0.30	0.003762
E13	Ca	Citr	0.1	0.60	0.41	0.00	0.00	0.00	0.001564
E13	Ca	Citr	0.3	0.29	0.71	0.00	0.00	0.00	0.006182
E13	Ca	Citr	0.6	0.00	0.92	0.07	0.00	0.02	0.005000
E13	Ca	Citr	2.4	-	-	-	-	-	-
E13	Ca	Citr	9.6	-	-	-	-	-	-
E13	Ca	LH	0.6	0.68	0.29	0.00	0.00	0.00	0.003007
E13	Ca	LH	2.4	0.53	0.36	0.00	0.00	0.02	0.002014
E13	Ca	LH	9.6	0.17	0.74	0.00	0.00	0.07	0.002485
E13	Na	Ctrl	0.0	0.79	0.09	0.05	0.00	0.00	0.011236
E15	Na	Ctrl	0.0	0.79	0.21	0.00	0.00	0.00	0.001098
E13	Na	2,4-DHB	0.6	0.80	0.17	0.02	0.00	0.00	0.000570
E13	Na	2,4-DHB	2.4	0.65	0.33	0.00	0.00	0.00	0.000538
E13	Na	2,4-DHB	9.6	0.31	0.67	0.00	0.00	0.00	0.000394
E13	Na	Galact	0.6	0.69	0.26	0.04	0.00	0.00	0.000589
E13	Na	Galact	2.4	0.38	0.62	0.00	0.00	0.00	0.005070
E13	Na	Galact	9.6	0.00	0.88	0.11	0.00	0.00	0.003303
E15	Na	3,4-DHB	0.6	0.13	0.77	0.00	0.00	0.02	0.002587
E15	Na	3,4-DHB	2.4	-	-	-	-	-	-
E15	Na	3,4-DHB	9.6	-	-	-	-	-	-
E13	Na	Citr	0.1	0.53	0.43	0.00	0.00	0.00	0.001209
E13	Na	Citr	0.3	0.12	0.81	0.00	0.02	0.03	0.001300
E13	Na	Citr	0.6	-	-	-	-	-	-
E13	Na	Citr	2.4	-	-	-	-	-	-
E13	Na	Citr	9.6	-	-	-	-	-	-
E13	Na	LH	0.6	0.69	0.16	0.02	0.00	0.00	0.000684
E13	Na	LH	2.4	0.26	0.75	0.00	0.00	0.00	0.001759
E13	Na	LH	9.6	0.01	0.92	0.00	0.04	0.00	0.005194

Table S7. LCF results for precipitates formed at $(P/Fe)_{init}$ 0.25

Experiment	Electrolyte	Organic	$(OC/Fe)_{init}$	Lp*	Fh*	FeP*	CaFeP*	FeOrg*	r-factor
E13	Ca	Ctrl	0.0	0.52	0.28	0.09	0.11	0.01	0.003145
E15	Ca	Ctrl	0.0	0.54	0.22	0.22	0.00	0.01	0.000680
E13	Ca	2,4-DHB	0.6	0.51	0.25	0.18	0.01	0.01	0.000637
E13	Ca	2,4-DHB	2.4	0.42	0.36	0.16	0.02	0.02	0.000482
E13	Ca	2,4-DHB	9.6	0.25	0.53	0.14	0.05	0.03	0.000294
E13	Ca	Galact	0.6	0.42	0.27	0.07	0.17	0.04	0.000825
E13	Ca	Galact	2.4	0.00	0.69	0.07	0.16	0.07	0.000568
E13	Ca	Galact	9.6	0.00	0.72	0.23	0.00	0.05	0.007873
E15	Ca	3,4-DHB	0.6	0.05	0.65	0.02	0.11	0.17	0.000712
E15	Ca	3,4-DHB	2.4	0.04	0.56	0.15	0.00	0.25	0.000906
E15	Ca	3,4-DHB	9.6	0.03	0.22	0.15	0.26	0.36	0.001610
E13	Ca	Citr	0.1	0.42	0.32	0.03	0.14	0.07	0.000705
E13	Ca	Citr	0.3	0.19	0.50	0.00	0.23	0.07	0.000440
E13	Ca	Citr	0.6	0.00	0.73	0.00	0.18	0.10	0.004232
E13	Ca	Citr	2.4	-	-	-	-	-	-
E13	Ca	Citr	9.6	-	-	-	-	-	-
E13	Ca	LH	0.6	0.45	0.11	0.01	0.27	0.01	0.007417
E13	Ca	LH	2.4	0.20	0.47	0.09	0.12	0.02	0.004015
E13	Ca	LH	9.6	0.05	0.59	0.00	0.18	0.14	0.001883
E13	Na	Ctrl	0.0	0.44	0.27	0.27	0.00	0.02	0.003070
E15	Na	Ctrl	0.0	0.45	0.21	0.33	0.00	0.00	0.000758
E13	Na	2,4-DHB	0.6	0.39	0.30	0.30	0.00	0.00	0.000705
E13	Na	2,4-DHB	2.4	0.30	0.38	0.31	0.00	0.00	0.000931
E13	Na	2,4-DHB	9.6	0.18	0.45	0.33	0.00	0.02	0.000516
E13	Na	Galact	0.6	0.31	0.29	0.36	0.00	0.02	0.001237
E13	Na	Galact	2.4	0.02	0.60	0.37	0.00	0.00	0.001267
E13	Na	Galact	9.6	0.01	0.43	0.43	0.00	0.10	0.001006
E15	Na	3,4-DHB	0.6	0.05	0.58	0.27	0.00	0.09	0.000587
E15	Na	3,4-DHB	2.4	-	-	-	-	-	-
E15	Na	3,4-DHB	9.6	-	-	-	-	-	-
E13	Na	Citr	0.1	0.17	0.71	0.12	0.00	0.00	0.010585
E13	Na	Citr	0.3	-	-	-	-	-	-
E13	Na	Citr	0.6	-	-	-	-	-	-
E13	Na	Citr	2.4	-	-	-	-	-	-
E13	Na	Citr	9.6	-	-	-	-	-	-
E13	Na	LH	0.6	0.22	0.43	0.25	0.00	0.01	0.002883
E13	Na	LH	2.4	0.06	0.66	0.00	0.11	0.08	0.002046
E13	Na	LH	9.6	0.00	0.62	0.00	0.19	0.16	0.019990

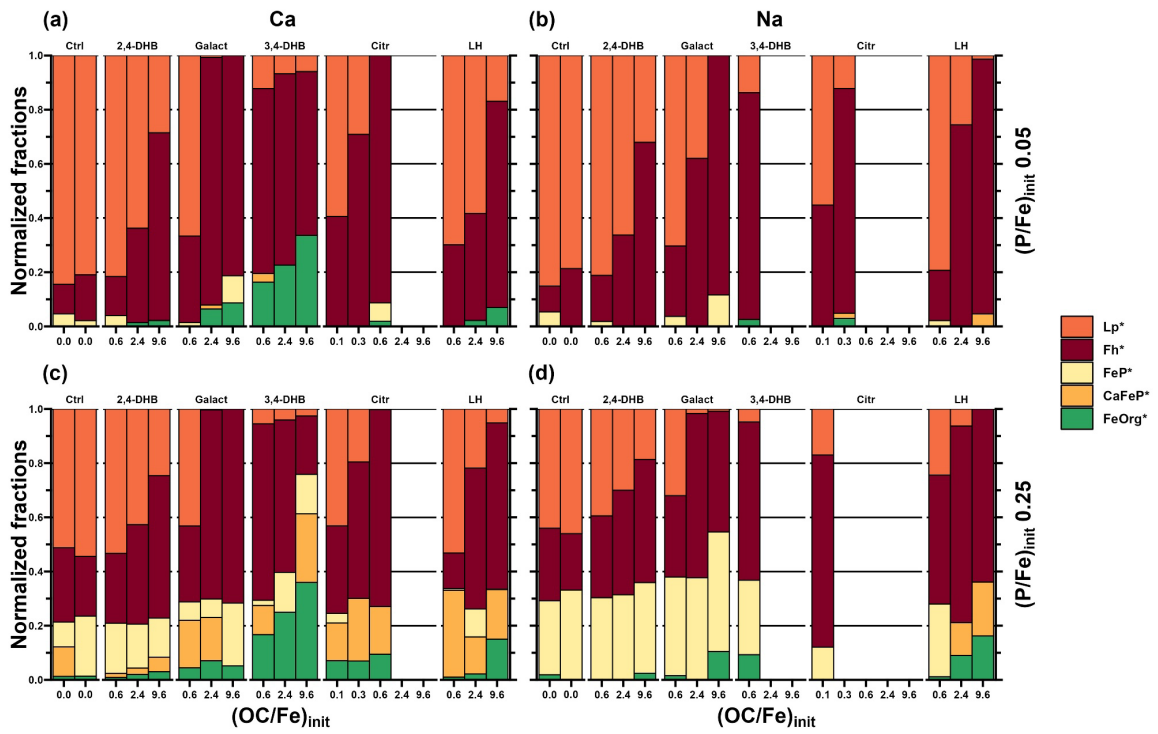


Figure S4. Fe K-edge EXAFS LCF results for solids recovered on 0.1- μm filter membranes.

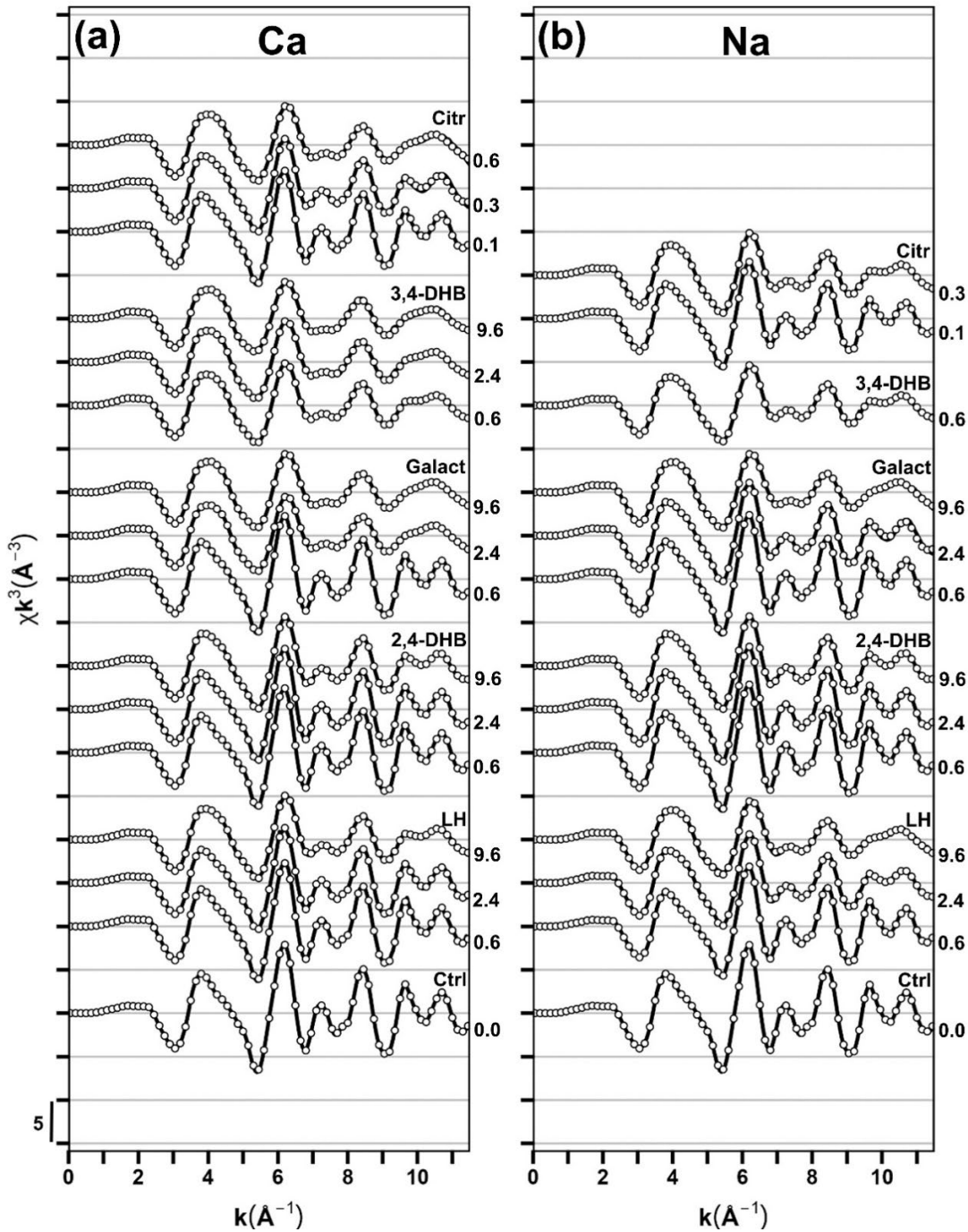


Figure S5. k^3 -weighted EXAFS spectra (solid lines) and reconstructed LCF fits (white circles) for precipitates formed in (a) Ca 0.05 and (b) Na 0.05 electrolytes. Numbers on the right side of the spectra indicate the $(\text{OC}/\text{Fe})_{\text{init}}$.

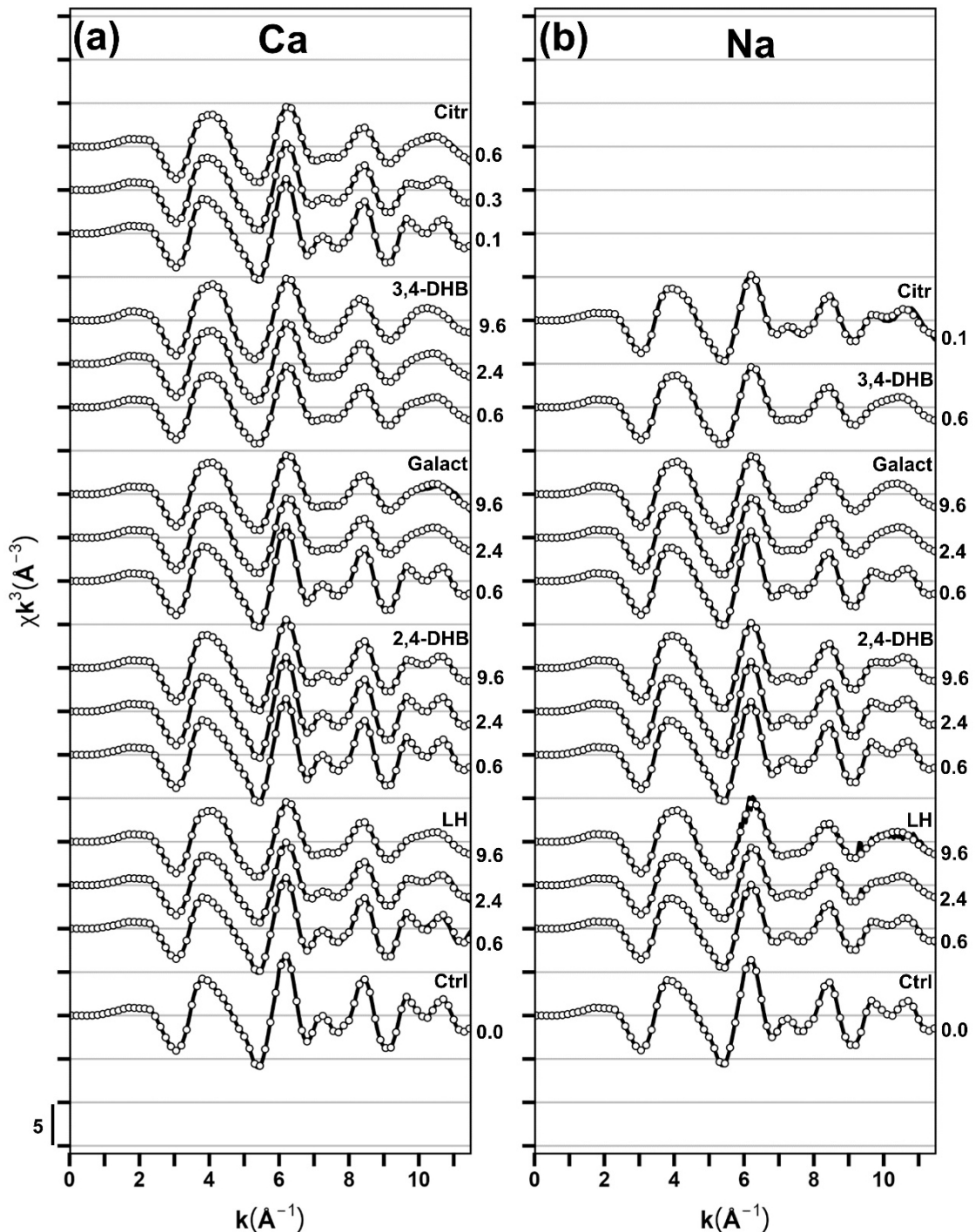


Figure S6. k^3 -weighted EXAFS spectra (solid lines) and reconstructed LCF fits (white circles) for precipitates formed in (a) Ca 0.25 and (b) Na 0.25 electrolytes. Numbers on the right side of the spectra indicate the $(\text{OC}/\text{Fe})_{\text{init.}}$

5 X-ray diffraction

Table S8. Full width at half maximum (FWHM) of (020) diffraction peak of Lp at 15.97° 2θ for precipitates formed in Ca and Na electrolytes at (P/Fe)_{init} 0.05 and 0.25 and the corresponding coherently scattering domain size (CSD) calculated using the Scherrer equation.

	(OC/Fe) _{init}	Ca				Na			
		(P/Fe) _{init} 0.05		(P/Fe) _{init} 0.25		(P/Fe) _{init} 0.05		(P/Fe) _{init} 0.25	
Organic		FWHM (°)	CSD (nm)						
Ctrl	0.0	7.23	1.29	11.5	0.81	6.02	1.55	10.27	0.91
LH	0.6	6.72	1.39	Lp ^a	Lp ^a	# ^d	# ^d	10.52	0.89
LH	2.4	10.3	0.90	Lp ^a	Lp ^a	# ^d	# ^d	Lp ^a	Lp ^a
LH	9.6	Lp ^a	Lp ^a	Lp ^a	Lp ^a	# ^d	# ^d	# ^d	# ^d
2,4-DHB	0.6	7.13	1.31	Lp ^a	Lp ^a	8.03	1.16	Lp ^a	Lp ^a
2,4-DHB	2.4	7.47	1.25	Lp ^a	Lp ^a	9.07	1.03	Lp ^a	Lp ^a
2,4-DHB	9.6	12.1	0.77	Lp ^a	Lp ^a	12.4	0.75	Lp ^a	Lp ^a
Galact	0.6	9.46	0.99	12.8	0.73	11.9	0.78	11.4	0.82
Galact	2.4	NLp ^b	NLp ^b	NLp ^b	NLp ^b	16.0	0.58	NLp ^b	NLp ^b
Galact	9.6	NLp ^b	NLp ^b						
3,4-DHB	0.1	-	-	-	-	6.13	1.52	13.5	0.69
3,4-DHB	0.3	-	-	-	-	9.71	0.96	Lp ^a	Lp ^a
3,4-DHB	0.6	8.49	1.10	NLp ^b	NLp ^b	NLp ^b	NLp ^b	Lp ^a	Lp ^a
3,4-DHB	2.4	NLp ^b	NLp ^b	NLp ^b	NLp ^b	NS ^c	NS ^c	NS ^c	NS ^c
3,4-DHB	9.6	NLp ^b	NLp ^b	NLp ^b	NLp ^b	NS ^c	NS ^c	NS ^c	NS ^c
Citr	0.1	8.01	1.16	Lp ^a	Lp ^a	# ^d	# ^d	Lp ^a	Lp ^a
Citr	0.3	10.3	0.91	Lp ^a	Lp ^a	NS ^c	NS ^c	NS ^c	NS ^c
Citr	0.6	NLp ^b	NLp ^b	NLp ^b	NLp ^b	NS ^c	NS ^c	NS ^c	NS ^c

^aLp without 020 peak identified in the diffraction pattern (Lp)

^bLp was not identified in the diffraction pattern (NLp)

^cNo solids on the membrane (NS)

^dSolids could not be removed from the membrane (#)

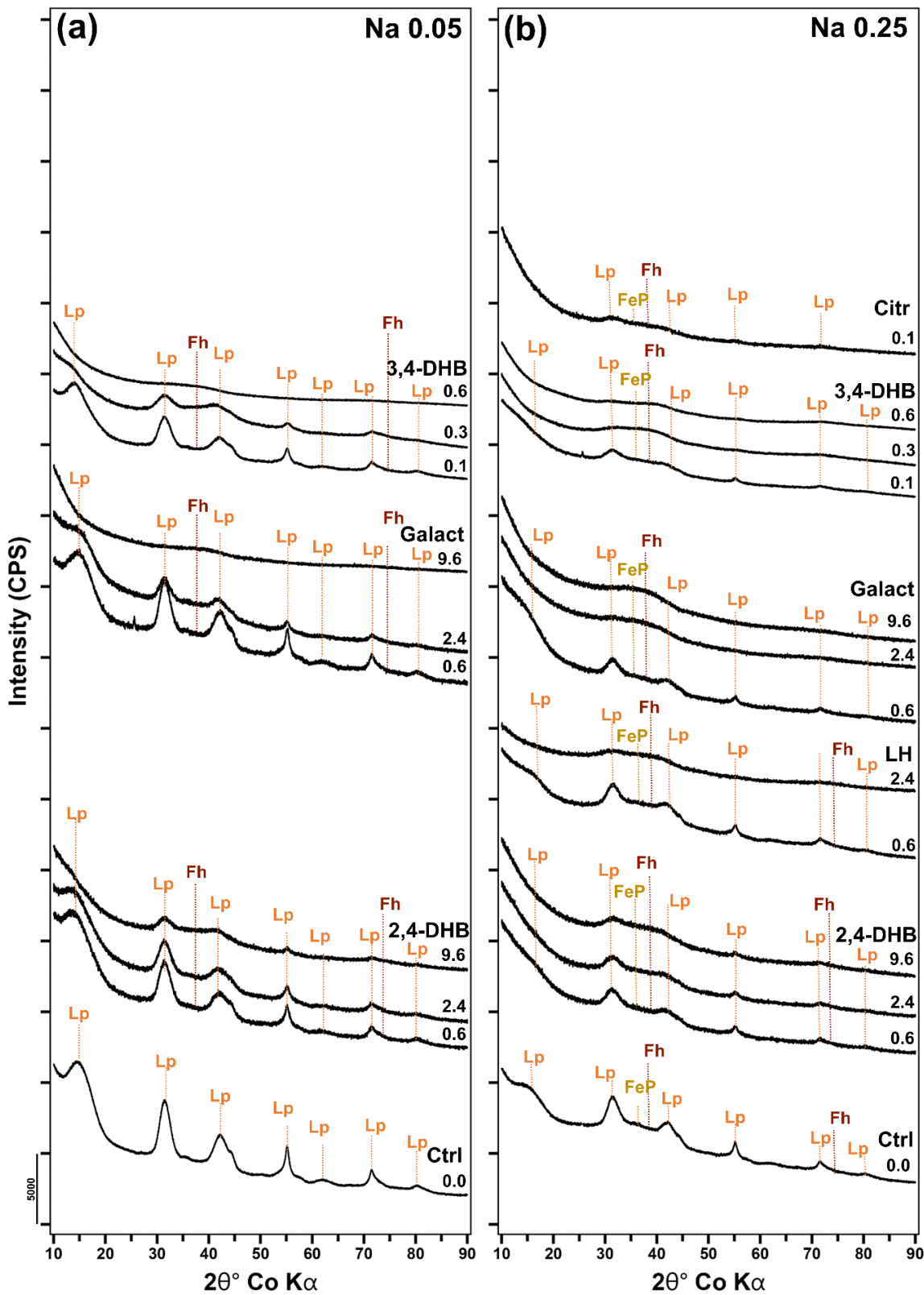


Figure S7. X-ray diffraction patterns of Fe-precipitates formed in Na background electrolytes at $(P/Fe)_{init}$ 0.05 (a) and 0.25 (b).

6 Fourier-transform infrared spectroscopy (FTIR)

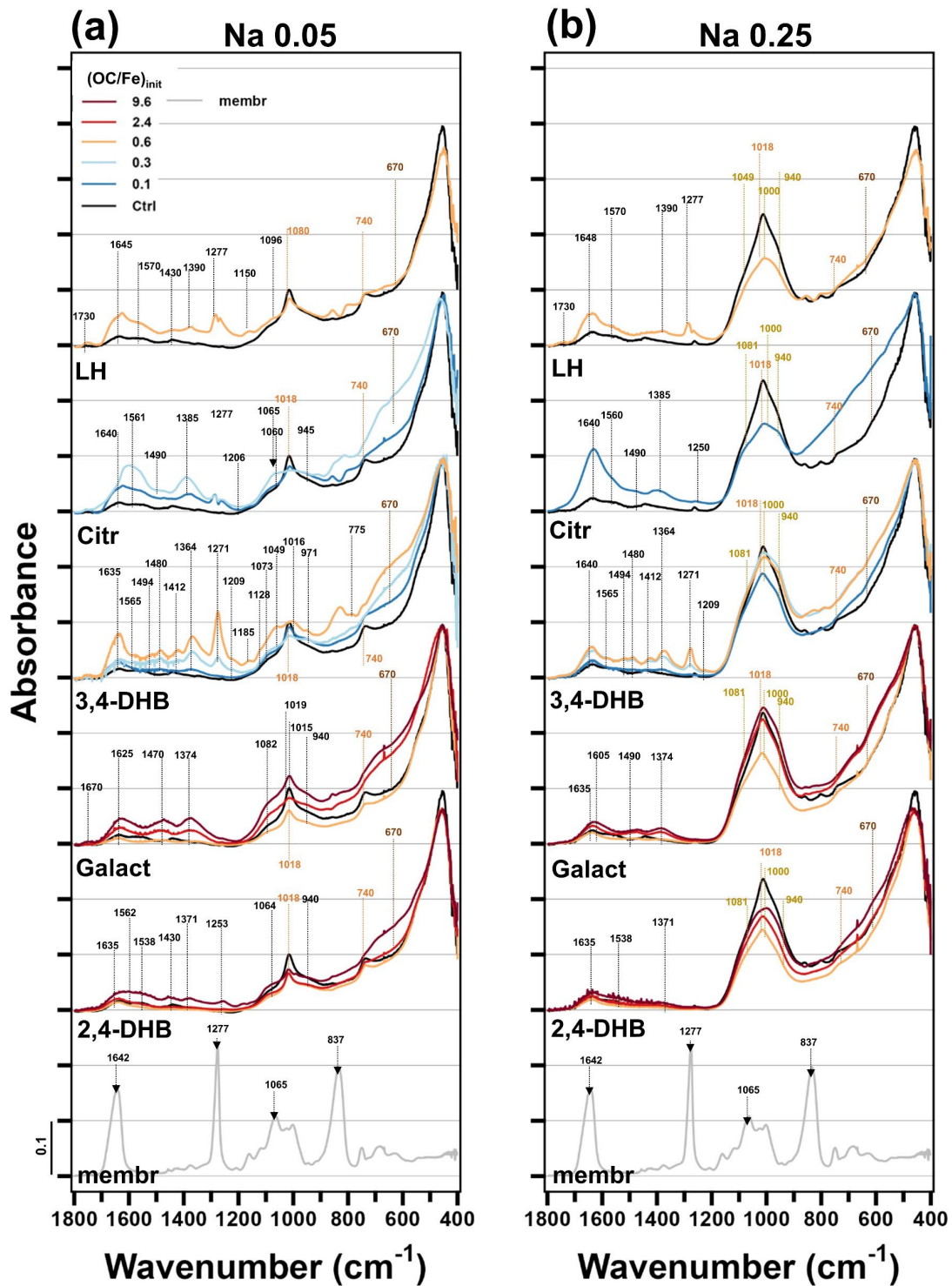


Figure S8. FTIR spectra of precipitates formed in Na electrolytes. Precipitates formed in the presence of LH and Citr at $(\text{P}/\text{Fe})_{\text{init}}$ 0.05 had to be measured on the cellulose nitrate filter membrane used for solids collection and contained spectral features from the membrane material that was subtracted from the sample spectra (cellulose nitrate membrane spectra are shown at bottom of panels).

7 Scanning transmission electron microscopy

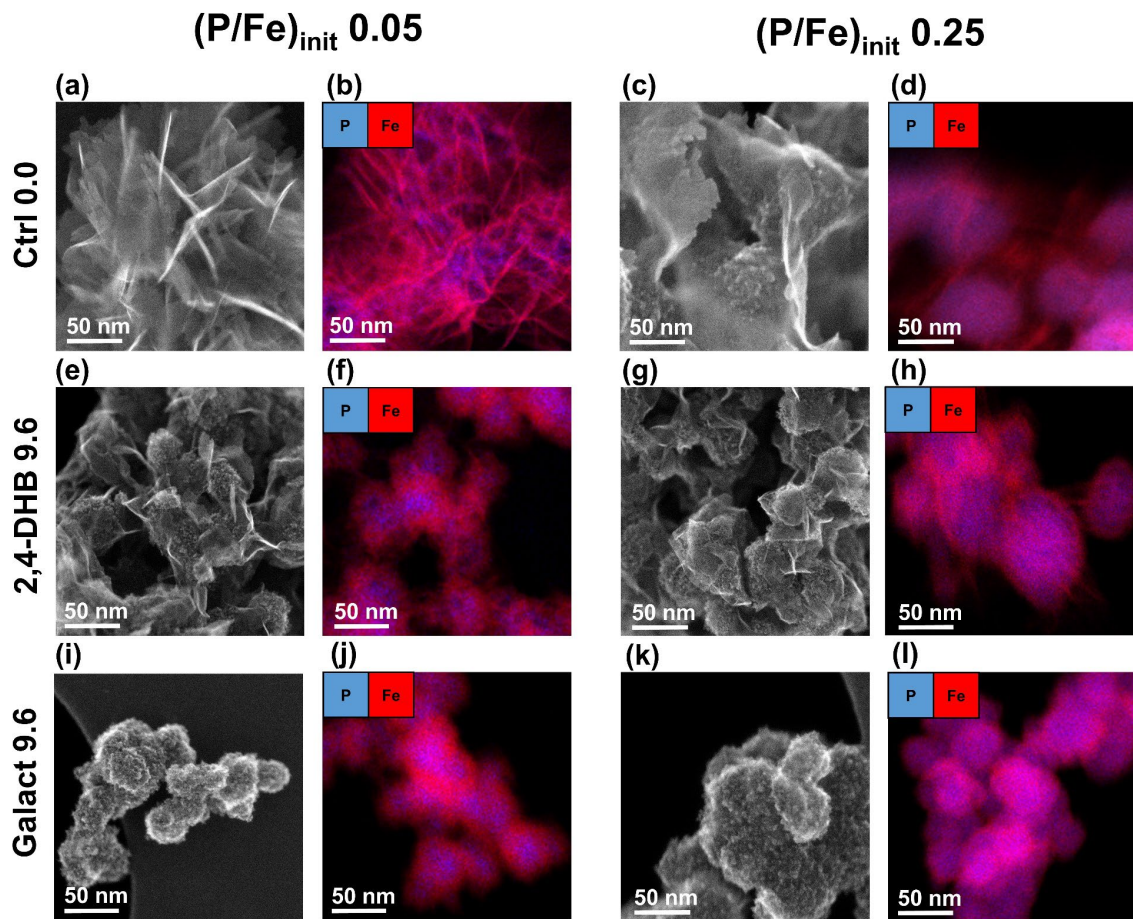


Figure S9. Secondary electron (SE) images of Fe(III)-precipitates formed in Na electrolytes at $(\text{P}/\text{Fe})_{\text{init}}$ of 0.05 (a,e,i) or 0.25 (c,g,k), and energy-dispersive X-ray (EDX) elemental distribution maps of P and Fe from the respective treatments at $(\text{P}/\text{Fe})_{\text{init}}$ of 0.05 (b,f,j) or 0.25 (d,h,l)- – for 2,4-DHB and Galact at $(\text{OC}/\text{Fe})_{\text{init}}$ 9.6.

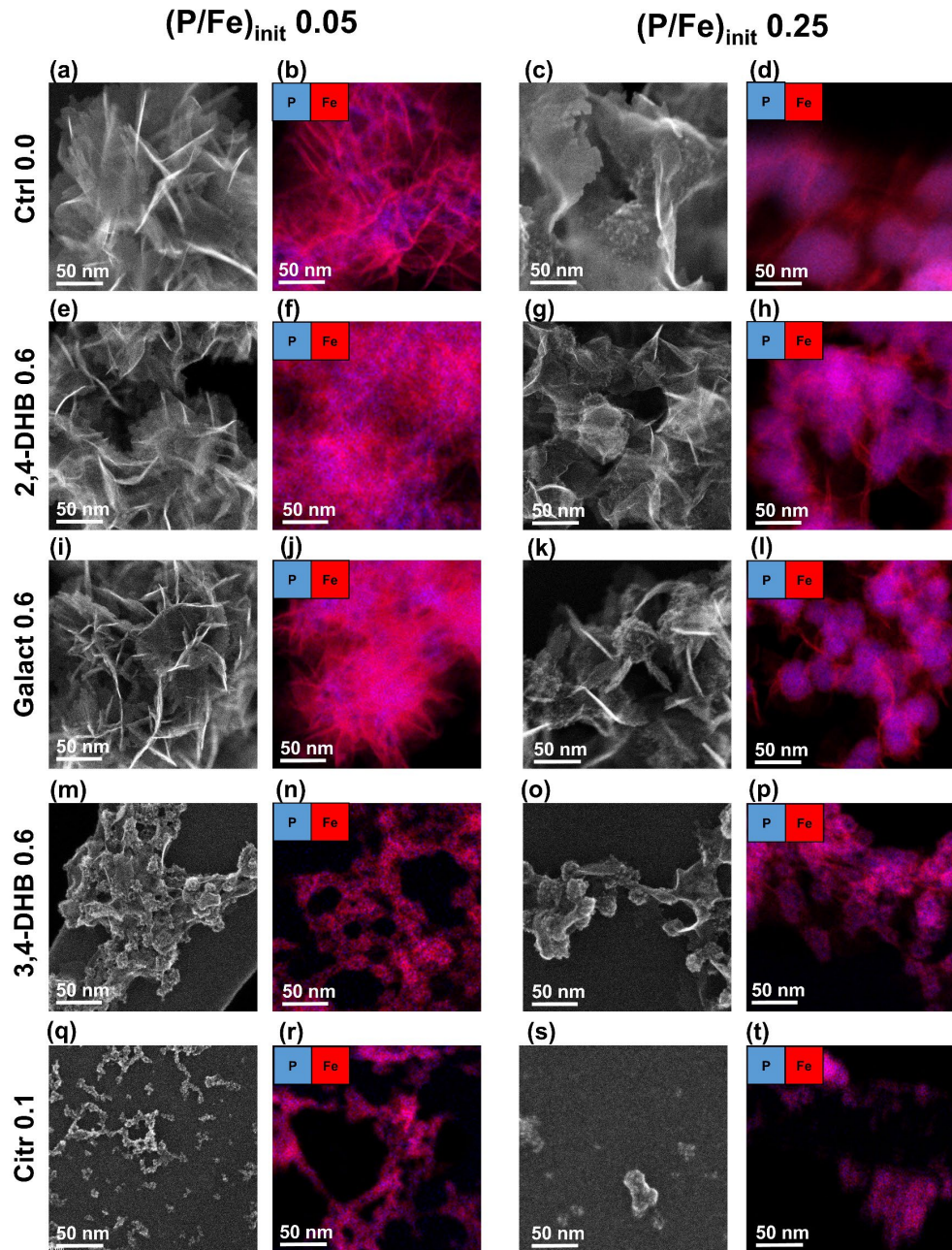


Figure S10. Secondary electron (SE) images of Fe(III)-precipitates formed in Na electrolytes at $(P/Fe)_{init}$ of 0.05 (a,e,i,m,q) or 0.25 (c,g,k,o,s) at $(OC/Fe)_{init}$ 0.6 or 0.1, and energy-dispersive X-ray (EDX) elemental distribution maps of P and Fe from the respective treatments at $(P/Fe)_{init}$ of 0.05 (b,f,j,n,r) or 0.25 (d,h,l,p,t) – for 2,4-DHB, Galact and 3,4-DHB at $(OC/Fe)_{init}$ 0.6 and for Citr at $(OC/Fe)_{init}$ 0.1.

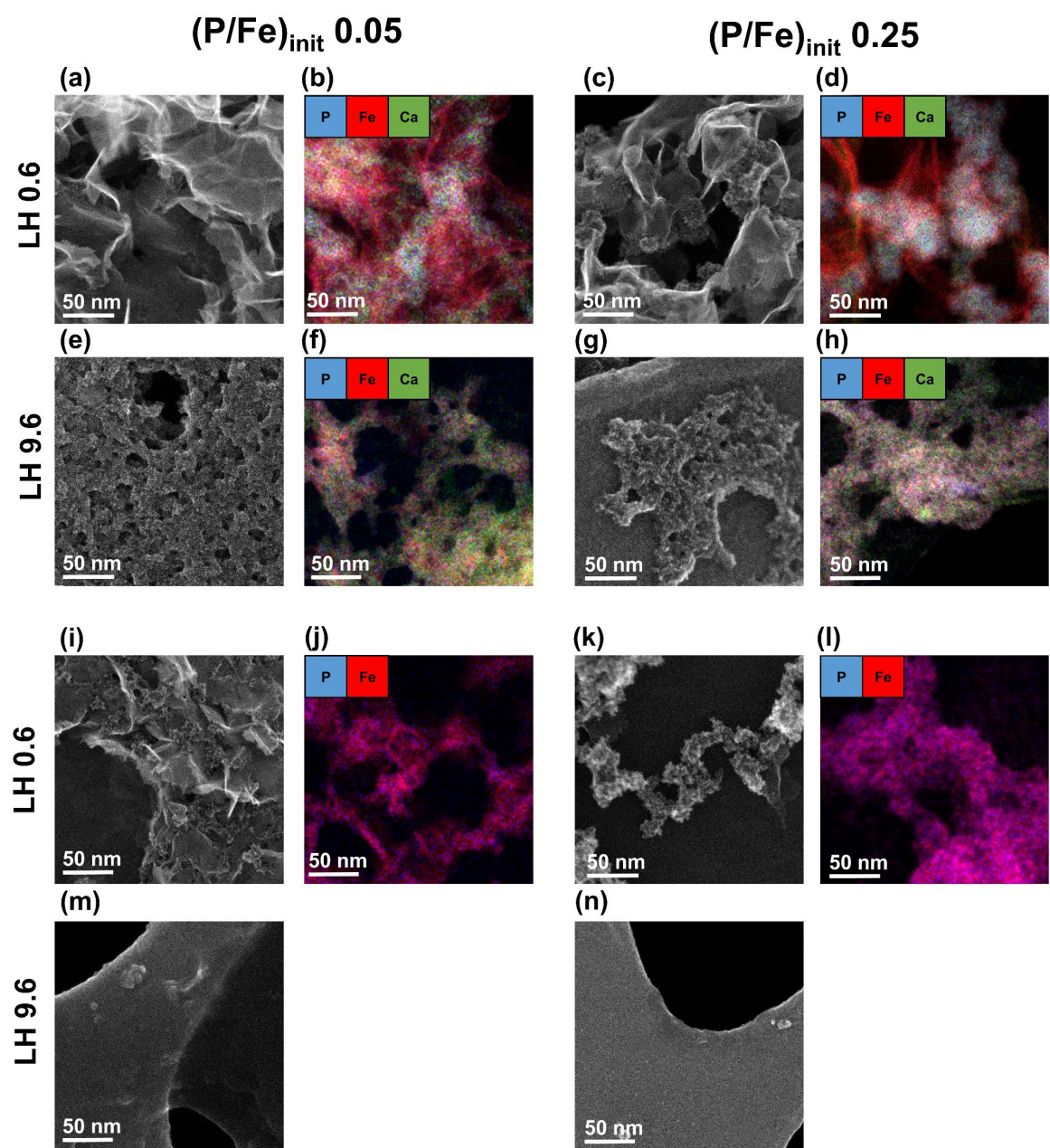


Figure S11. Secondary electron (SE) images and EDX element distribution maps ((Ca), Fe, P) of Fe(III)-precipitates formed in presence of LH in Ca and Na electrolytes: Ca 0.05 LH 0.6 (a,b), Ca 0.25 LH 0.6 (c,d), Ca 0.05 LH 9.6 (e,f), Ca 0.25 LH 9.6 (g,h), Na 0.05 LH 0.6 (i,j), Na 0.25 LH 0.6 (k,l), Na 0.05 LH 9.6 (m, EDX not analyzed) and Na 0.25 LH 9.6 (n, EDX not analyzed).

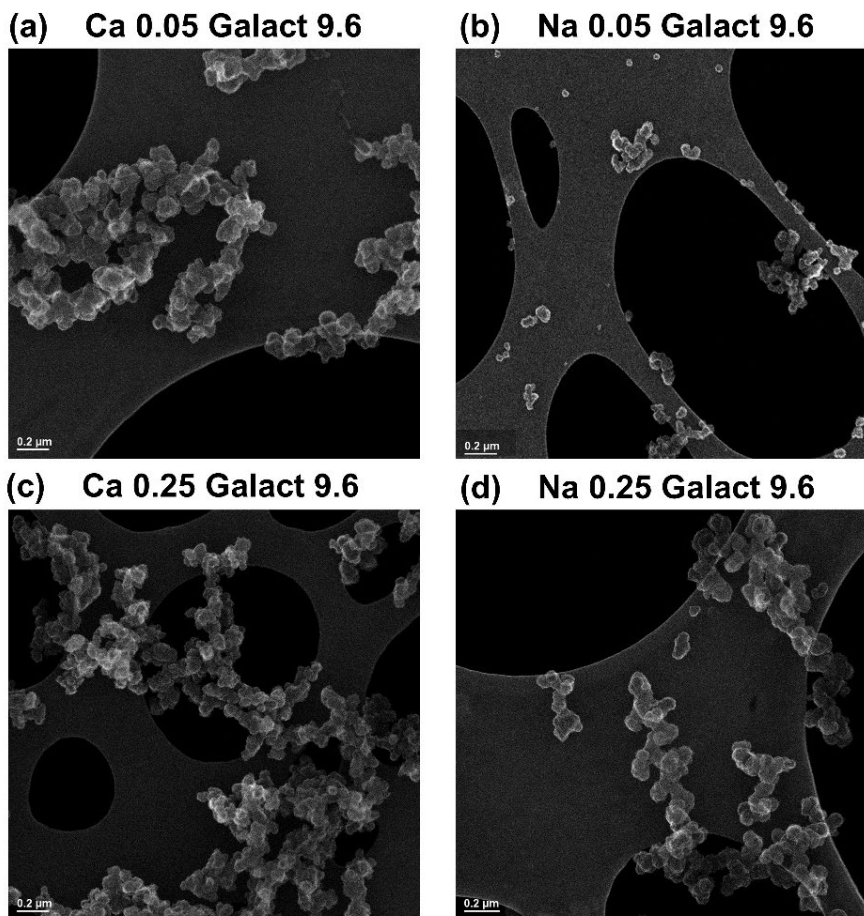


Figure S12. Secondary electron images at lower magnification for Fe(III)-precipitates formed in the presence of Galact at $(\text{OC}/\text{Fe})_{\text{init}}$ 9.6 in Ca and Na electrolytes. At both $(\text{P}/\text{Fe})_{\text{init}}$, precipitates formed in the absence of Ca consisted of smaller and less aggregated particles.

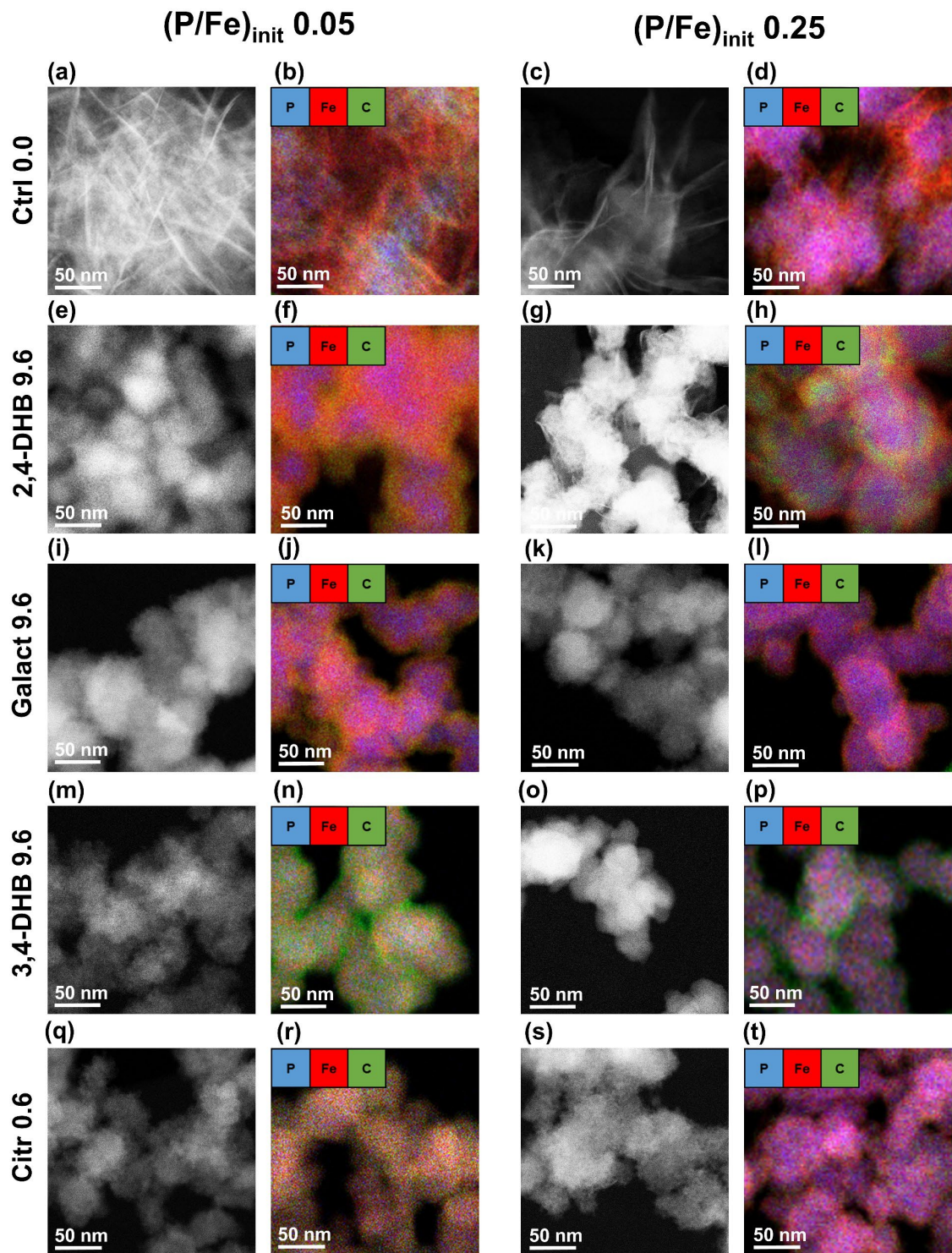


Figure S13. High-angle annular dark-field (HAADF) images of Fe(III)-precipitates formed in Ca electrolytes at $(\text{P}/\text{Fe})_{\text{init}}$ of 0.05 (a,e,i,m,q) or 0.25 (c,g,k,o,s), and energy-dispersive X-ray (EDX) elemental distribution maps of P, Fe, and C from the respective treatments at $(\text{P}/\text{Fe})_{\text{init}}$ of 0.05 (b,f,j,n,r) or 0.25 (d,h,l,p,t) – for 2,4-DHB, Galact and 3,4-DHB at $(\text{OC}/\text{Fe})_{\text{init}}$ 9.6 and for Citr at $(\text{OC}/\text{Fe})_{\text{init}}$ 0.6.

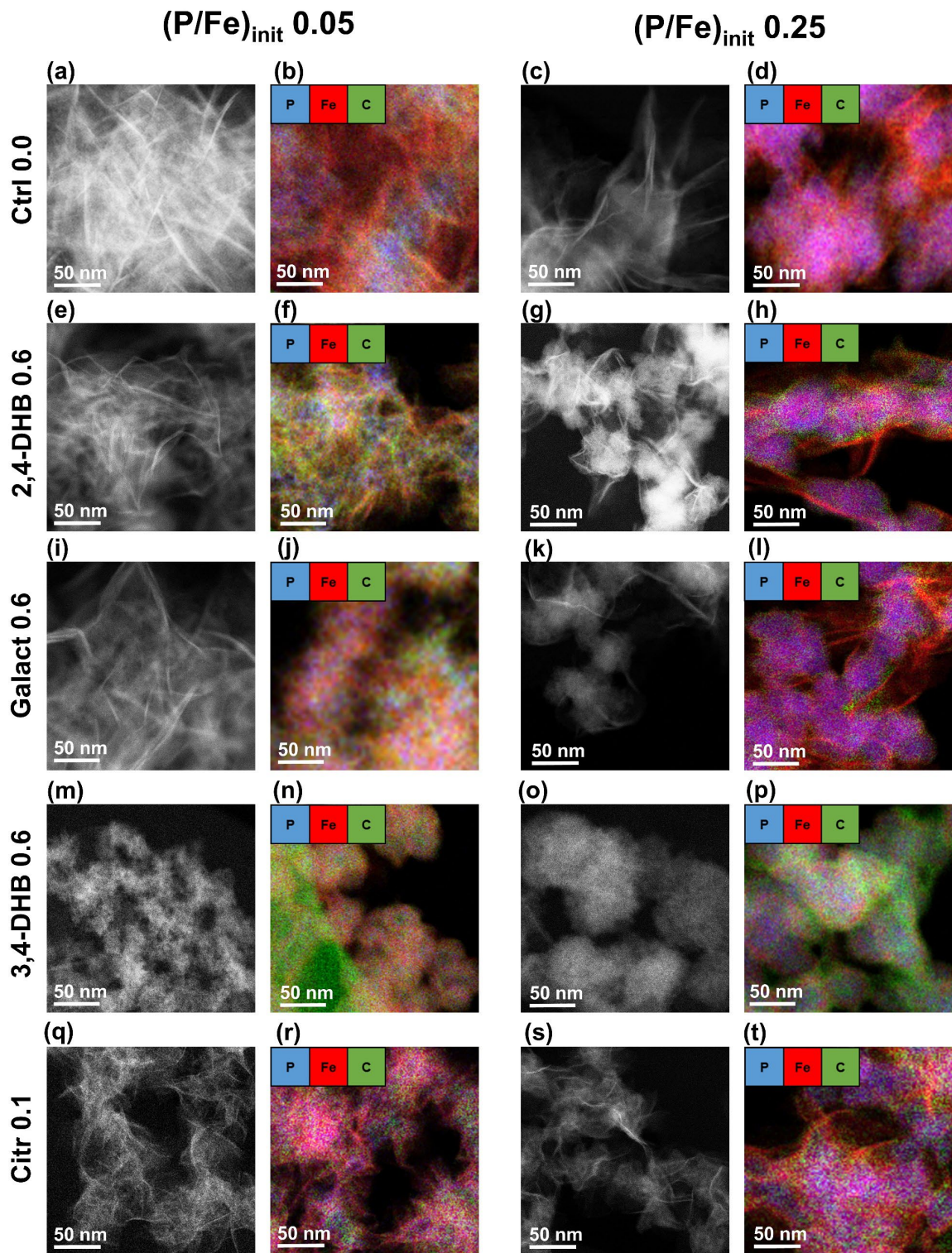


Figure S14. High-angle annular dark-field (HAADF) images of Fe(III)-precipitates formed in Ca electrolytes at $(\text{P}/\text{Fe})_{\text{init}}$ of 0.05 (a,e,i,m,q) or 0.25 (c,g,k,o,s), and energy-dispersive X-ray (EDX) elemental distribution maps of P, Fe, and C from the respective treatments at $(\text{P}/\text{Fe})_{\text{init}}$ of 0.05 (b,f,j,n,r) or 0.25 (d,h,l,p,t) – for 2,4-DHB, Galact and 3,4-DHB at $(\text{OC}/\text{Fe})_{\text{init}}$ 0.6 and for Citr at $(\text{OC}/\text{Fe})_{\text{init}}$ 0.1.

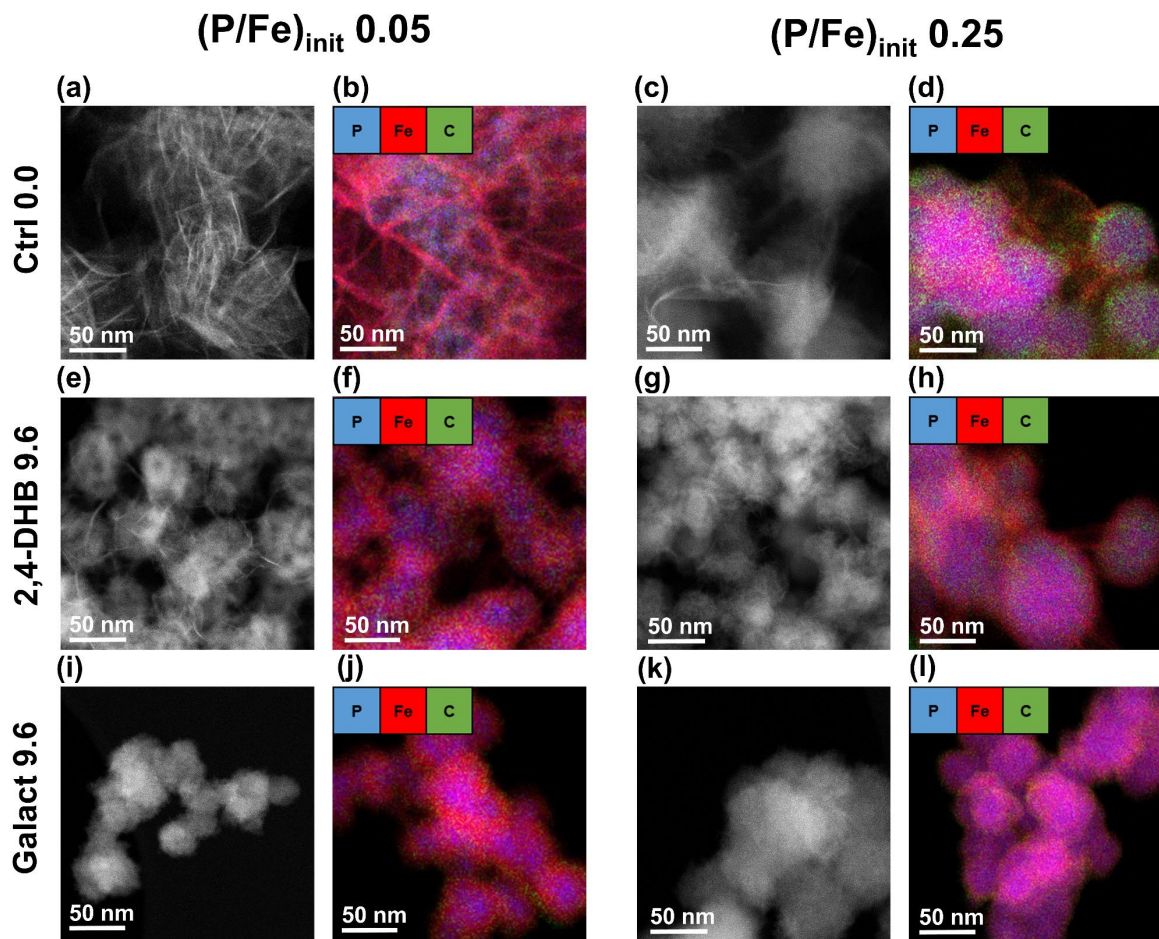


Figure S15. High-angle annular dark-field (HAADF) images of Fe(III)-precipitates formed in Na electrolytes at $(\text{P}/\text{Fe})_{\text{init}}$ of 0.05 (a,e,i) or 0.25 (c,g,k), and energy-dispersive X-ray (EDX) elemental distribution maps of P, Fe, and C from the respective treatments at $(\text{P}/\text{Fe})_{\text{init}}$ of 0.05 (b,f,j) or 0.25 (d,h,l) – for 2,4-DHB and Galact at $(\text{OC}/\text{Fe})_{\text{init}}$ 9.6.

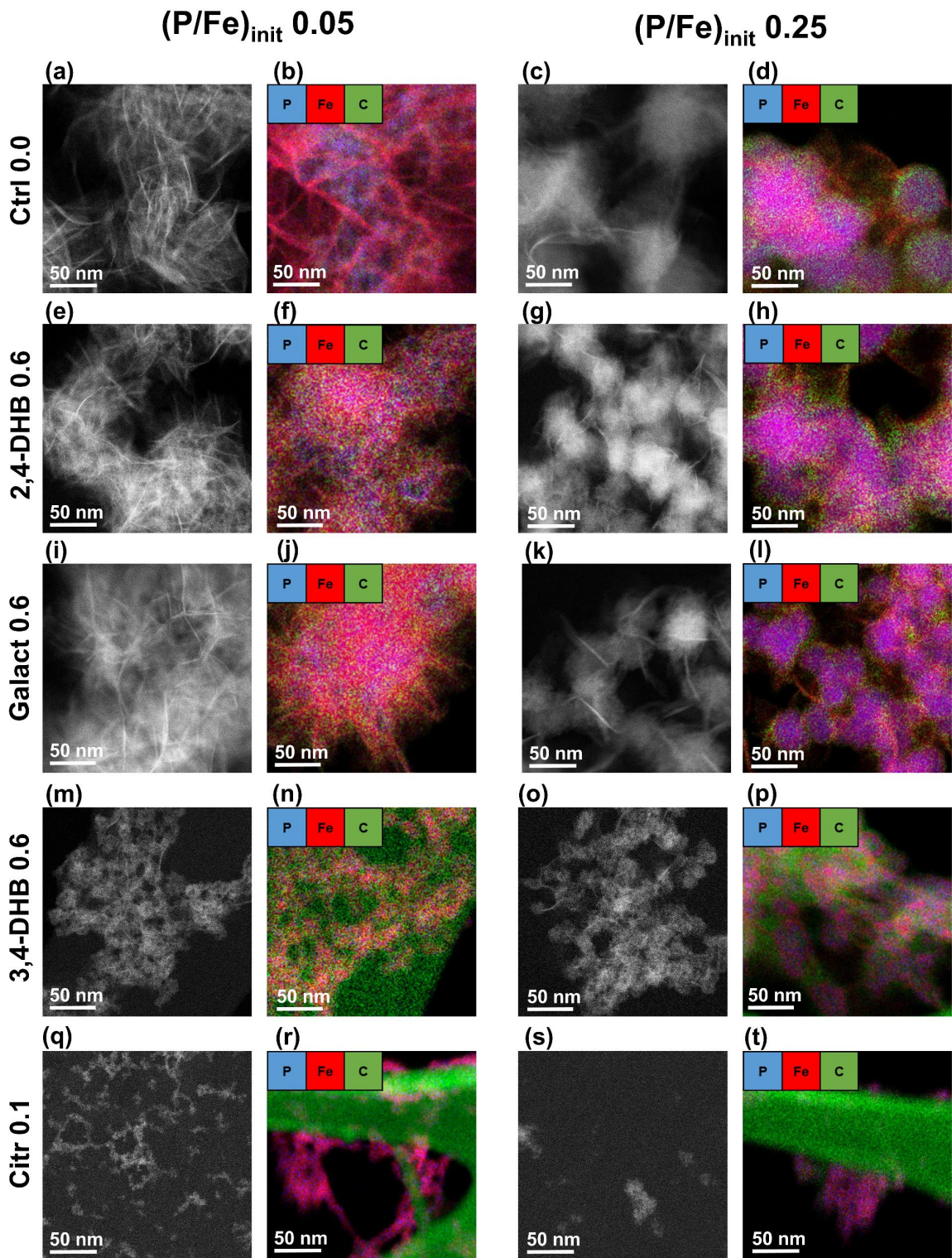


Figure S16. High-angle annular dark-field (HAADF) images of Fe(III)-precipitates formed in Na electrolytes at (P/Fe)_{init} of 0.05 (a,e,i,m,q) or 0.25 (c,g,k,o,s), and energy-dispersive X-ray (EDX) elemental distribution maps of P, Fe, and C from the respective treatments at (P/Fe)_{init} of 0.05 (b,f,j,n,r) or 0.25 (d,h,l,p,t) – for 2,4-DHB, Galact and 3,4-DHB at (OC/Fe)_{init} 0.6 and for Citr at (OC/Fe)_{init} 0.1.

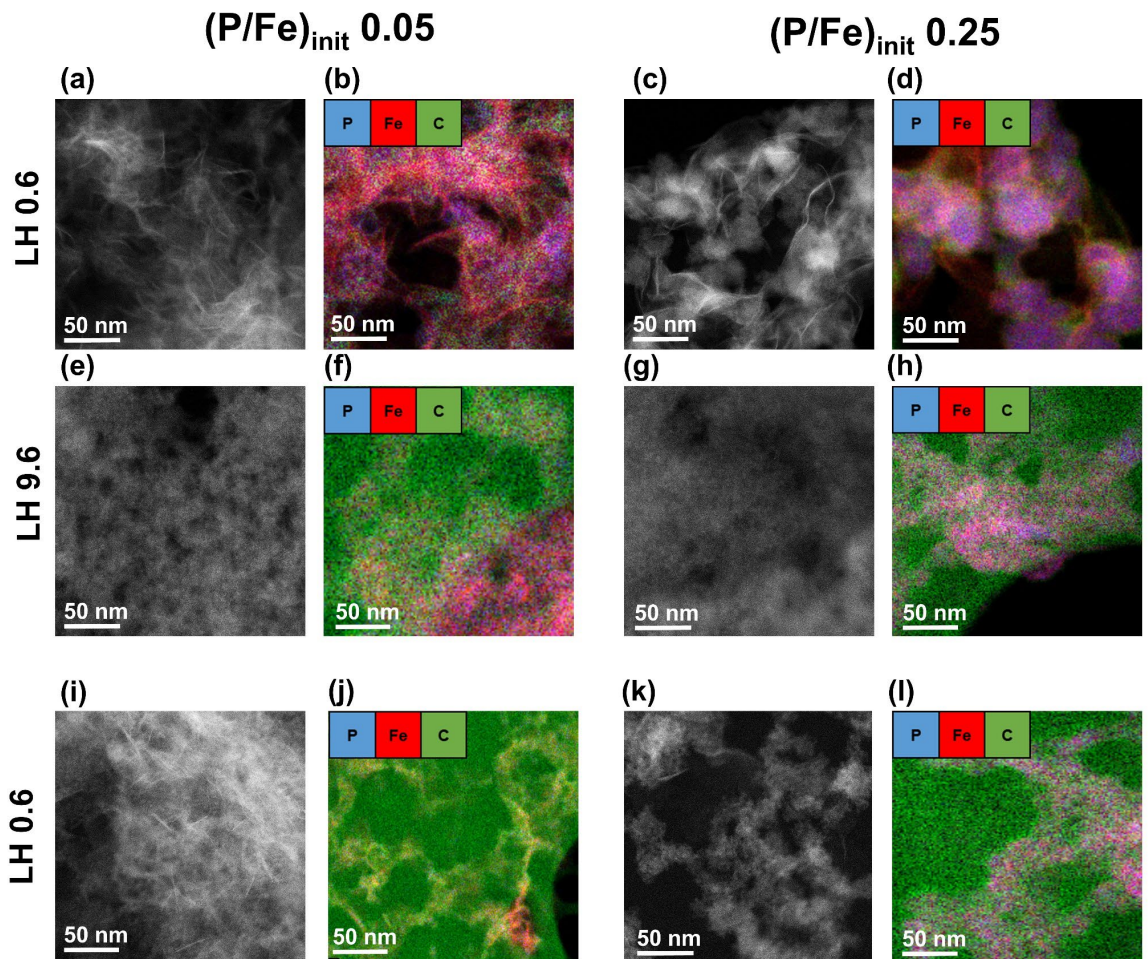


Figure S17. High-angle annular dark-field (HAADF) images and EDX element distribution maps (Fe, P, C) of Fe(III)-precipitates formed in the presence of LH in Ca and Na electrolytes: Ca 0.05 LH 0.6 (a,b), Ca 0.25 LH 0.6 (c,d), Ca 0.05 LH 9.6 (e,f), Ca 0.25 LH 9.6 (g,h), Na 0.05 LH 0.6 (i,j) and Na 0.25 LH 0.6 (k,l).

Table S9. Elemental ratios derived from STEM-EDX analyses on precipitates formed in Ca electrolytes.

Organic	$(OC/Fe)_{init}$	$(P/Fe)_{init} 0.05$											
		entire imaged area (~bulk)			high-P particle cores (~Fh)			low-P particle shells (~Fh)			sheets / platelets (Lp)		
		(P/Fe)	(TC/Fe)	(Ca/Fe)	(P/Fe)	(TC/Fe)	(Ca/Fe)	(P/Fe)	(TC/Fe)	(Ca/Fe)	(P/Fe)	(TC/Fe)	(Ca/Fe)
Ctrl	0.0	0.04	0.22	0.05	NI ^a	NI ^a	NI ^a	0.05	0.23	0.05	0.02	0.05	0.02
LH	0.6	0.05	1.41	0.05	0.05	1.34	0.05	NI ^a	NI ^a	NI ^a	0.04	1.09	0.02
LH	9.6	0.04	# ^b	0.22	NI ^a	NI ^a	NI ^a	0.04	# ^b	0.20	NI ^a	NI ^a	NI ^a
2,4-DHB	0.6	0.05	0.44	0.04	0.09	0.52	0.07	NI ^a	NI ^a	NI ^a	0.03	0.26	0.01
2,4-DHB	9.6	0.04	0.63	0.06	0.10	0.29	0.11	0.01	0.62	0.04	NI ^a	NI ^a	NI ^a
Galact	0.6	0.05	0.36	0.00	0.05	0.98	0.00	0.03	1.08	0.00	NI ^a	NI ^a	NI ^a
Galact	9.6	0.07	0.67	0.08	0.15	0.47	0.12	0.02	0.63	0.05	NI ^a	NI ^a	NI ^a
3,4-DHB	0.6	0.05	1.29	0.10	0.06	1.64	0.11	0.03	1.23	0.09	NI ^a	NI ^a	NI ^a
3,4-DHB	9.6	0.10	4.82	0.19	0.12	4.19	0.21	0.07	9.48	0.16	NI ^a	NI ^a	NI ^a
Citr	0.1	0.03	1.13	0.01	0.05	1.27	0.02	NI ^a	NI ^a	NI ^a	0.03	1.09	0.01
Citr	0.6	0.05	1.68	0.11	0.06	0.76	0.12	NI ^a	NI ^a	NI ^a	NI ^a	NI ^a	NI ^a
Organic	$(OC/Fe)_{init}$	$(P/Fe)_{init} 0.25$											
		entire imaged area (~bulk)			high-P particle cores (~CaFeP)			low-P particle shells (~Fh)			sheets / platelets (Lp)		
		(P/Fe)	(TC/Fe)	(Ca/Fe)	(P/Fe)	(TC/Fe)	(Ca/Fe)	(P/Fe)	(TC/Fe)	(Ca/Fe)	(P/Fe)	(TC/Fe)	(Ca/Fe)
Ctrl	0.0	0.23	0.26	0.25	0.39	0.28	0.30	0.12	0.28	0.08	0.03	0.19	0.04
LH	0.6	0.31	1.25	0.23	0.55	1.25	0.32	0.15	2.13	0.09	0.06	0.74	0.04
LH	9.6	0.28	# ^b	0.24	NI ^a	NI ^a	NI ^a	0.28	# ^b	0.23	NI ^a	NI ^a	NI ^a
2,4-DHB	0.6	0.31	0.41	0.19	0.45	0.25	0.30	0.17	0.85	0.09	0.04	0.56	0.01
2,4-DHB	9.6	0.26	0.25	0.14	0.43	0.27	0.22	0.22	0.43	0.12	0.05	0.12	0.06
Galact	0.6	0.25	0.29	0.20	0.42	0.32	0.33	0.13	0.43	0.11	0.03	0.35	0.04
Galact	9.6	0.32	0.45	0.20	0.44	0.38	0.25	0.08	0.86	0.08	NI ^a	NI ^a	NI ^a
3,4-DHB	0.6	0.25	1.60	0.19	0.33	1.38	0.24	0.12	2.26	0.09	NI ^a	NI ^a	NI ^a
3,4-DHB	9.6	0.52	4.81	0.41	0.53	3.42	0.41	0.43	19.95	0.59	NI ^a	NI ^a	NI ^a
Citr	0.1	0.23	0.41	0.09	0.43	2.62	0.15	0.06	1.45	0.02	NI ^a	NI ^a	NI ^a
Citr	0.6	0.26	0.83	0.24	0.31	0.81	0.27	0.15	0.91	0.16	NI ^a	NI ^a	NI ^a

^aphase not identified with EDX (NI)

^boverlap by the carbon grid (#)

Table S10. Elemental ratios derived from EDX measurements from precipitates formed in Na electrolytes.

Organic	$(OC/Fe)_{init}$	$(P/Fe)_{init} 0.05$							
		entire imaged area (~bulk)		high-P particle cores (~Fh)		low-P particle shells (~Fh)		sheets / platelets (Lp)	
		(P/Fe)	(TC/Fe)	(P/Fe)	(TC/Fe)	(P/Fe)	(TC/Fe)	(P/Fe)	(TC/Fe)
Ctrl	0.0	0.04	0.09	NI ^a	NI ^a	0.04	0.25	0.02	0.00
LH	0.6	0.04	# ^b	NI ^a	NI ^a	0.05	# ^b	NI ^a	NI ^a
LH	9.6	NS ^c	NS ^c	NS ^c	NS ^c	NS ^c	NS ^c	NS ^c	NS ^c
2,4-DHB	0.6	0.04	0.22	0.06	0.15	NI ^a	NI ^a	0.04	0.20
2,4-DHB	9.6	0.05	0.35	0.09	0.34	NI ^a	NI ^a	0.03	0.36
Galact	0.6	0.05	0.47	0.06	0.35	0.05	0.72	0.03	0.63
Galact	9.6	0.07	0.25	0.13	0.11	0.02	0.26	NI ^a	NI ^a
3,4-DHB	0.6	0.06	# ^b	NI ^a	NI ^a	0.06	# ^b	NI ^a	NI ^a
3,4-DHB	9.6	NS ^c	NS ^c	NS ^c	NS ^c	NS ^c	NS ^c	NS ^c	NS ^c
Citr	0.3	0.06	0.59	NI ^a	NI ^a	0.05	0.49	NI ^a	NI ^a
Citr	0.6	NS ^c	NS ^c	NS ^c	NS ^c	NS ^c	NS ^c	NS ^c	NS ^c
Organic	$(OC/Fe)_{init}$	$(P/Fe)_{init} 0.25$							
		entire imaged area (~bulk)		high-P particle cores (~FeP)		low-P particle shells (~Fh)		sheets / platelets (Lp)	
		(P/Fe)	(TC/Fe)	(P/Fe)	(TC/Fe)	(P/Fe)	(TC/Fe)	(P/Fe)	(TC/Fe)
Ctrl	0.0	0.19	0.17	0.37	0.30	NI ^a	NI ^a	0.07	0.23
LH	0.6	0.25	# ^b	NI ^a	NI ^a	NI ^a	NI ^a	NI ^a	NI ^a
LH	9.6	NS ^c	NS ^c	NS ^c	NS ^c	NS ^c	NS ^c	NS ^c	NS ^c
2,4-DHB	0.6	0.32	0.84	0.39	0.55	0.13	1.35	0.06	0.82
2,4-DHB	9.6	0.23	0.64	0.37	0.38	0.12	0.70	NI ^a	NI ^a
Galact	0.6	0.26	0.58	0.39	0.34	0.15	0.83	0.05	0.71
Galact	9.6	0.28	0.12	0.34	0.03	0.14	0.38	NI ^a	NI ^a
3,4-DHB	0.6	0.19	2.56	0.25	2.27	0.14	5.31	NI ^a	NI ^a
3,4-DHB	9.6	NS ^c	NS ^c	NS ^c	NS ^c	NS ^c	NS ^c	NS ^c	NS ^c
Citr	0.1	0.26	# ^b	NI ^a	NI ^a	NI ^a	NI ^a	NI ^a	NI ^a
Citr	0.6	NS ^c	NS ^c	NS ^c	NS ^c	NS ^c	NS ^c	NS ^c	NS ^c

^aphase not identified with EDX (NI)

^boverlap by the carbon grid (#)

^cno solids on the grid (NS)

8 Dynamic light scattering

Table S11. DLS results for aggregates formed in Ca 0.05 and 0.25 electrolytes: Average hydrodynamic aggregate diameter (Z ; in nm; standard deviation from triplicate independent experiments, where available), derived count rate (in counts per second) as qualitative indicator of particle concentration, and polydispersity index (PDI) as measure of aggregate polydispersity. The derived count rate and PDI are presented from a single experiment (E15). Gray shade indicates results with high PDI (>0.7), where aggregate polydispersity decreased the reliability of the measurement.

(P/Fe) _{init} 0.05				
Organic	(OC/Fe) _{init}	Z (nm)	derived count rate	PDI
Ctrl	0.0	2724 ± 807	36006	0.45
2,4-DHB	0.1	3040	57304	0.28
2,4-DHB	0.3	3003	35514	0.32
2,4-DHB	0.6	2663 ± 338	36091	0.46
2,4-DHB	1.2	2775 ± 120	44820	0.32
2,4-DHB	2.4	3277 ± 1003	65746	0.46
2,4-DHB	4.8	2654	71874	0.25
2,4-DHB	9.6	5291 ± 2720	104598	0.72
Galact	0.1	2405	42755	0.80
Galact	0.3	2721	17699	0.29
Galact	0.6	2295 ± 377	44109	0.50
Galact	1.2	2399 ± 117	56305	0.28
Galact	2.4	2265 ± 675	99489	0.46
Galact	4.8	1775	106113	0.29
Galact	9.6	1832 ± 642	99053	0.49
3,4-DHB	0.6	28030	53595	0.77
3,4-DHB	2.4	2192	75008	0.43
3,4-DHB	9.6	2444	4837	0.42
Citr	0.1	5004 ± 3064	40886	0.56
Citr	0.3	3892 ± 2310	67572	0.42
Citr	0.6	1581 ± 447	66854	0.38
Citr	2.4	1634	461	0.73
Citr	9.6	13	66	0.82
LH	0.1	3319	48021	0.60
LH	0.3	3681	44372	0.71
LH	0.6	2956 ± 1025	45136	0.46
LH	1.2	3769 ± 469	43100	0.58
LH	2.4	5756 ± 3812	41456	0.46
LH	4.8	2080	39493	1.00
LH	9.6	2260 ± 245	17442	0.89

Table S11. Continued.

(P/Fe) _{init} 0.25				
Organic	(OC/Fe) _{init}	Z (nm)	derived count rate	PDI
Ctrl	0.0	1678 ± 545	77499	0.62
2,4-DHB	0.6	2734 ± 1045	35862	0.83
2,4-DHB	2.4	3384 ± 1344	38546	0.52
2,4-DHB	9.6	5672	63121	0.89
Galact	0.6	2832 ± 696	41735	0.70
Galact	2.4	2300 ± 81	66827	0.59
Galact	9.6	2131	110408	0.75
3,4-DHB	0.6	4490	70407	0.49
3,4-DHB	2.4	1989	73446	0.43
3,4-DHB	9.6	1510	5971	0.27
Citr	0.1	5479	85907	0.89
Citr	0.3	5459	65436	0.90
Citr	0.6	1375 ± 949	44813	0.31
Citr	2.4	300	950	0.71
Citr	9.6	52	112	0.76
LH	0.6	3139 ± 1172	40274	0.55
LH	2.4	3117 ± 1212	35075	0.54
LH	9.6	3826	37800	0.31

Table S12. DLS results for aggregates formed in Na 0.05 and Na 0.25 electrolytes: Average hydrodynamic aggregate diameter (Z; in nm; standard deviation from triplicate independent experiments, where available), derived count rate (in counts per second) as qualitative indicator of particle concentration, and polydispersity index (PDI) as measure of aggregate polydispersity. Gray shade indicates results with high PDI (>0.7), where aggregate polydispersity decreased the reliability of the measurement. The derived count rate and PDI are presented from a single experiment (E15).

(P/Fe) _{init} 0.05				
Organic	(OC/Fe) _{init}	Z(nm)	derived count rate (cps)	PDI
Ctrl	0.0	2559 ± 126	28866	0.21
2,4-DHB	0.3	1847	36689	0.26
2,4-DHB	0.6	1793 ± 39	53098	0.46
2,4-DHB	1.2	1999	51843	0.25
2,4-DHB	2.4	1993 ± 724	59591	0.41
2,4-DHB	9.6	8275	54136	0.83
Galact	0.3	2058	42705	0.25
Galact	0.6	1255 ± 459	66824	0.22
Galact	1.2	1423	65286	0.27
Galact	2.4	763 ± 455	92440	0.25
Galact	9.6	1152 ± 997	107715	0.45
3,4-DHB	0.6	9545	7388	0.70
3,4-DHB	2.4	36	904	0.25
3,4-DHB	9.6	162	22	0.29
Citr	0.1	3630	47539	0.84
Citr	0.3	799	7955	0.25
Citr	0.6	49	815	0.46
Citr	2.4	137	136	0.43
Citr	9.6	9	36	0.61
LH	0.6	12247 ± 13167	26314	0.60
LH	1.2	1105	13728	0.42
LH	2.4	145 ± 37	12671	0.29
LH	9.6	159	9567	0.53
(P/Fe) _{init} 0.25				
Organic	(OC/Fe) _{init}	Z (nm)	derived count rate	PDI
Ctrl	0.0	1129	77790	0.33
2,4-DHB	0.6	1474 ± 1401	40829	0.44
2,4-DHB	2.4	1272 ± 1210	41728	0.48
2,4-DHB	9.6	5662	101527	0.59
Galact	0.6	705 ± 562	50259	0.33
Galact	2.4	222 ± 146	42966	0.32
Galact	9.6	162	95489	0.13
3,4-DHB	0.6	163	19190	0.25
3,4-DHB	2.4	46	1967	0.19
3,4-DHB	9.6	9	40712	0.47
Citr	0.1	1335	13123	0.79
Citr	0.3	222	137726	0.14
Citr	0.6	58	750	0.52
Citr	2.4	37	188	0.87
Citr	9.6	17	66	0.75
LH	0.6	693 ± 378	10212	0.75
LH	2.4	168 ± 67	6595	0.35
LH	9.6	146	10521	0.53

9 Turbidity

The turbidity of unfiltered suspensions was examined over a period of 24 hours upon resuspension. The initial turbidity values, expressed in Nephelometric Turbidity Units (NTUs), along with the time required to achieve a 50% decrease in turbidity ($t_{50\%}$), and the remaining turbidity as a percentage after 24 hours, are presented in Table S13. The measurements up to the 24-h revealed that the presence of organic ligands had a noticeable impact on the rate of turbidity reduction when compared to the control.

In the case of Ca electrolytes, turbidity measurements after 24 hours indicated effective particle removal through sedimentation in all suspensions. At Ca 0.25 treatments, the higher PO₄ concentration increased the time of turbidity removal. The organic ligands generally increased the time of turbidity reduction and the sedimentation times with increasing (OC/Fe)_{init}. Notably, exceptions were observed in the cases of 2,4-DHB and 3,4-DHB, where the rate of turbidity decrease increased. For 2,4-DHB, the rate of turbidity decrease increased with increasing (OC/Fe)_{init}. For suspensions containing 3,4-DHB at (OC/Fe)_{init} 0.6 at both (P/Fe)_{init}, the rate of turbidity decrease was higher than in Ctrl. Additionally in these treatments, the presence of visible flocs was observed, as depicted in Figure S19.

In the case of Na electrolytes, the organic ligands significantly decreased the rate of turbidity removal. Notable exceptions were with all 2,4-DHB treatments and 3,4-DHB at (P/Fe)_{init} 0.05, where the rate of turbidity decrease increased. Furthermore, in most of the Galact, 3,4-DHB, and Citr treatments, most of the suspensions retained nearly 100% of turbidity after 24 hours, suggesting colloidal stabilization. Photographs in Figure S19b (for Galact), S20b (for 3,4-DHB), and S21b (for Citr), further illustrate that these suspensions remained characterized by high turbidity after 24 h. Moreover, in the case of 3,4-DHB the solution during oxidation turned blue, indicating dissolved Fe(III)-catecholate complexes.

Regarding the LH, in Ca-electrolytes, with increasing (OC/Fe)_{init}, the rate of turbidity decrease increased and the particles were observed to settle over time, forming dark flocs (Fig S22a). On the other hand, in Na electrolytes, Fe and LH formed flocs only at (OC/Fe)_{init} 0.6, and at higher (OC/Fe)_{init}, the particles remained colloidally stable, as indicated by photographs in Figure S22b.

Table S13. Turbidity results.

		Ca						Na					
		(P/Fe) _{init}						(P/Fe) _{init}					
Organic	(OC/Fe) _{init}	0.05			0.25			0.05			0.25		
		NTU _{0h}	NTU _{24h (%)}	t _{(50%) (h)}	NTU _{0h}	NTU _{24h (%)}	t _{(50%) (h)}	NTU _{0h}	NTU _{24h (%)}	t _{(50%) (h)}	NTU _{0h}	NTU _{24h (%)}	t _{(50%) (h)}
Ctrl	0.0	116	4%	1.6	127	5%	1.9	137	4%	1.5	158	5%	1.6
2,4-DHB	0.6	184	5%	4.1	169	5%	3.4	188	8%	8.9	173	13%	8.5
	2.4	202	6%	4.0	189	6%	3.2	182	8%	5.5	155	10%	7.5
	9.6	265	6%	2.9	206	7%	5.4	106	5%	2.7	113	7%	4.3
Galact	0.6	209	3%	2.5	152	4%	3.5	120	12%	15	115	96%	69
	2.4	261	6%	4.9	194	3%	4.8	125	94%	76	132	97%	# ^a
	9.6	273	7%	9.2	14	9%	15	81	100%	# ^a	120	100%	# ^a
3,4-DHB	0.6	124	3%	0.5	107	5%	3.6	20	7%	0.4	25	100%	# ^a
	2.4	99	6%	5.5	91	7%	5.8	0.5	100%	# ^a	1.0	97%	# ^a
	9.6	11	14%	15	14	9%	15	0.0	90%	# ^a	0.0	100%	# ^a
Citr	0.1	158	1%	2.5	182	1%	2.2	26	7%	1.7	24	60%	30
	0.3	181	1%	2.2	233	1%	1.7	7.0	100%	# ^a	1.1	100%	# ^a
	0.6	83	1%	4.1	113	1%	3.7	1.1	100%	# ^a	0.3	100%	# ^a
LH	0.6	113	5%	3.7	127	2%	3.1	35	11%	2.2	40	54%	79
	2.4	87	2%	1.8	85	3%	2.6	19	94%	# ^a	12	92%	# ^a
	9.6	90	3%	1.4	105	2%	1.0	11	94%	# ^a	12	93%	# ^a

^a t_(50%) could not be determined (#).

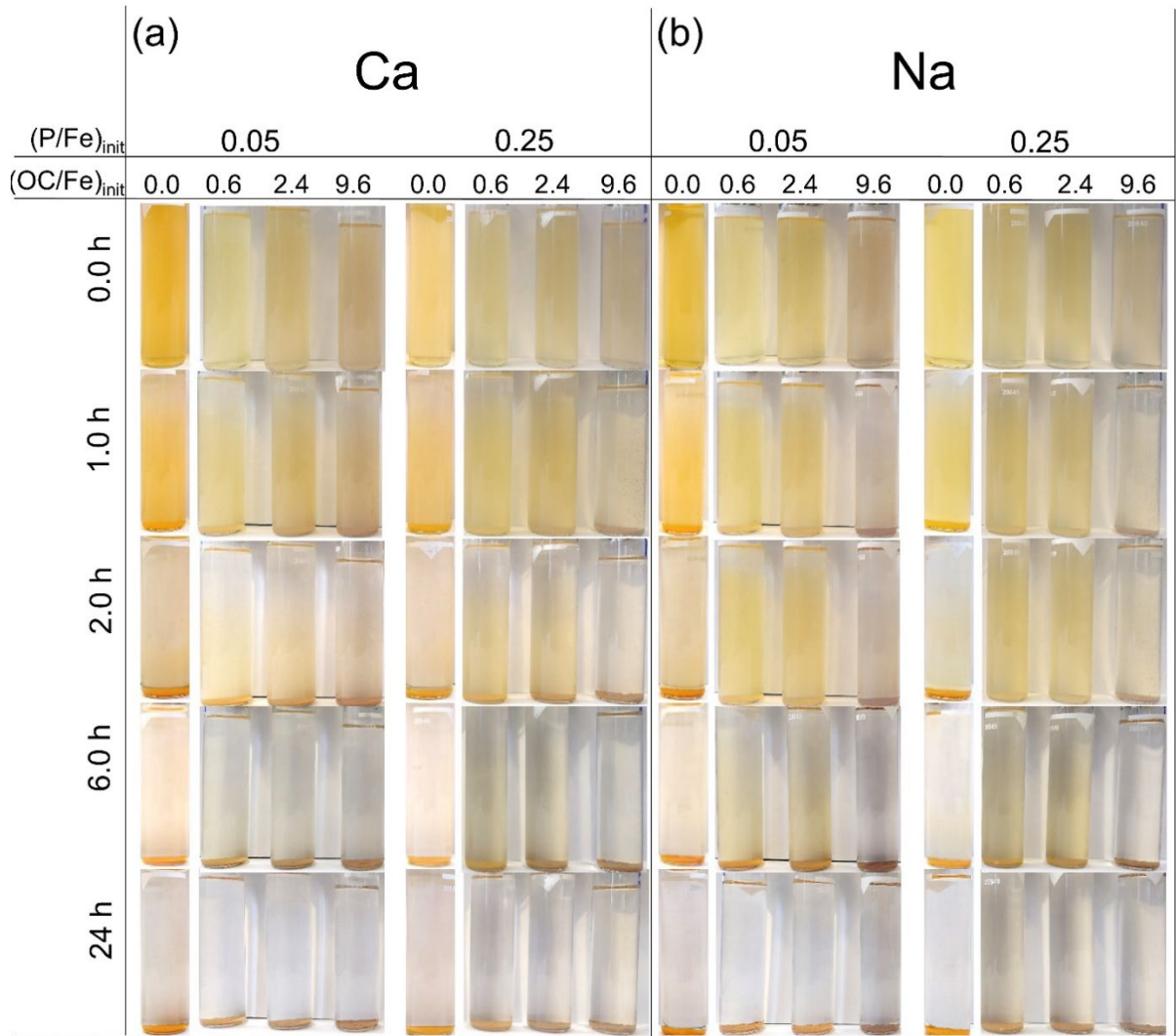


Figure S18. Photos of precipitate suspensions formed in presence of 2,4-DHB; over 24-h settling period upon dispersion.

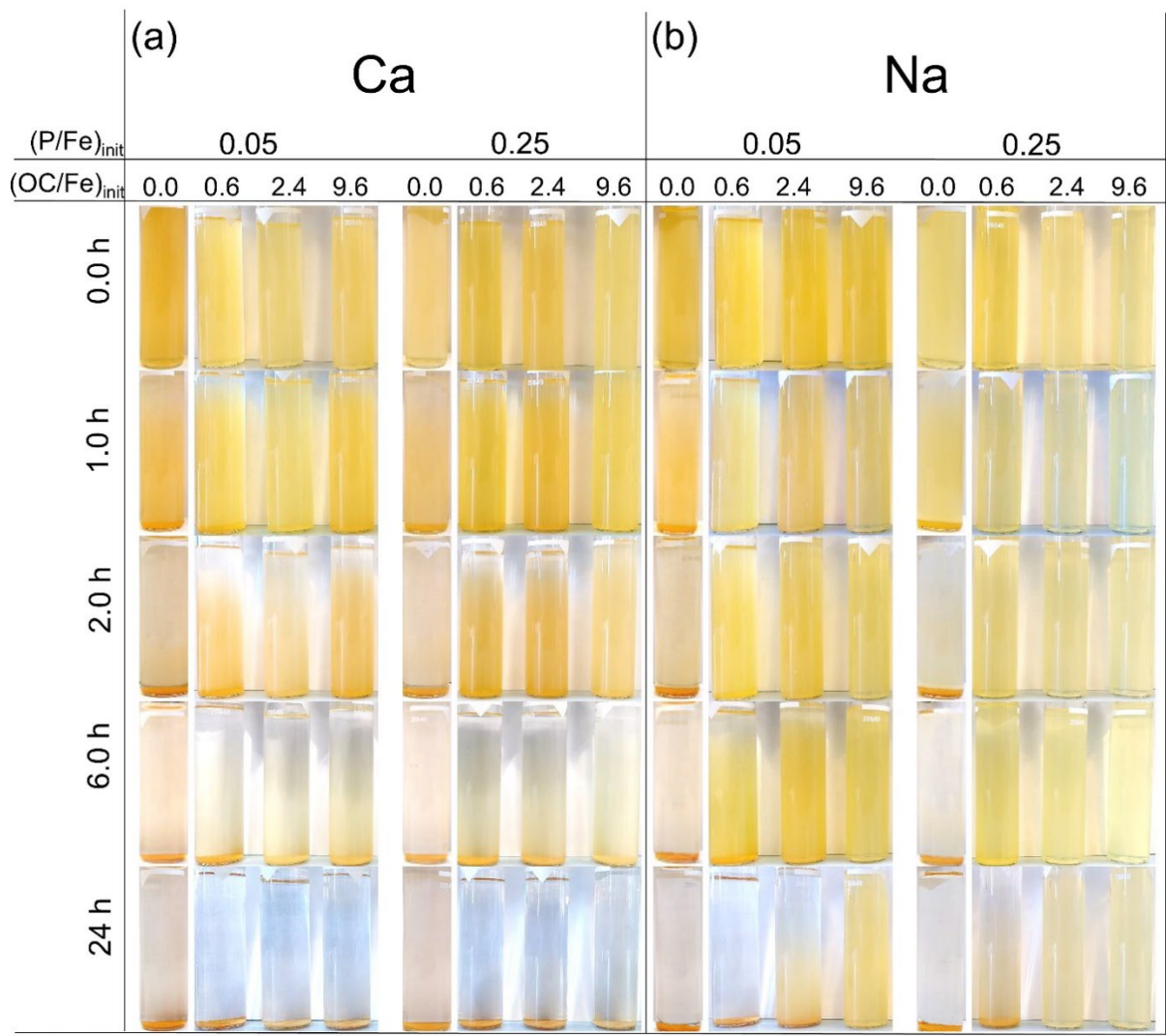


Figure S19. Photos of precipitate suspensions formed in presence of Galact; over 24-h settling period upon re-dispersion.

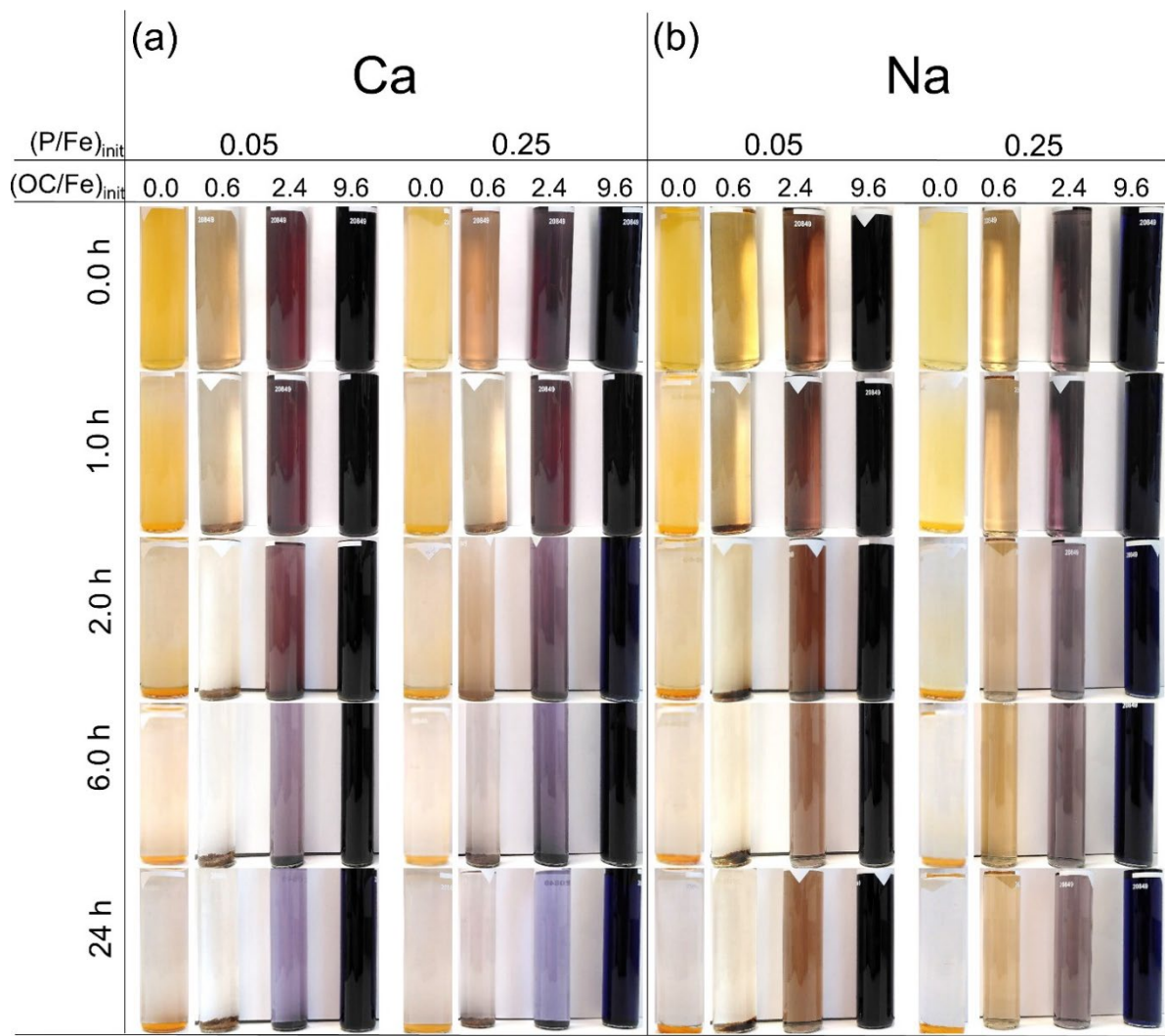


Figure S20. Photos of precipitate suspensions formed in presence of 3,4-DHB; over 24-h settling period upon re-dispersion.

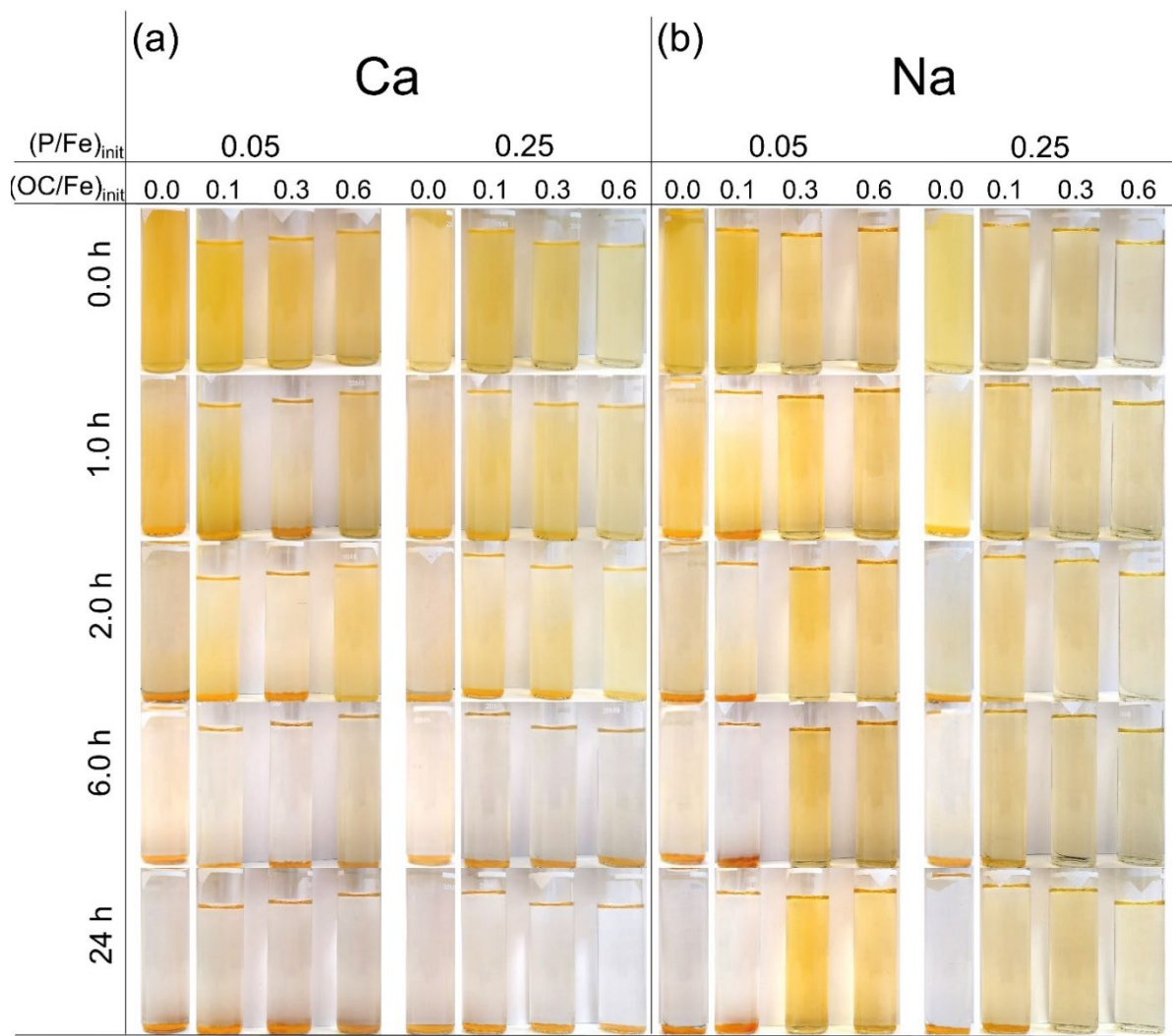


Figure S21. Photos of precipitate suspensions formed in presence of Citr; over 24-h settling period upon re-dispersion.

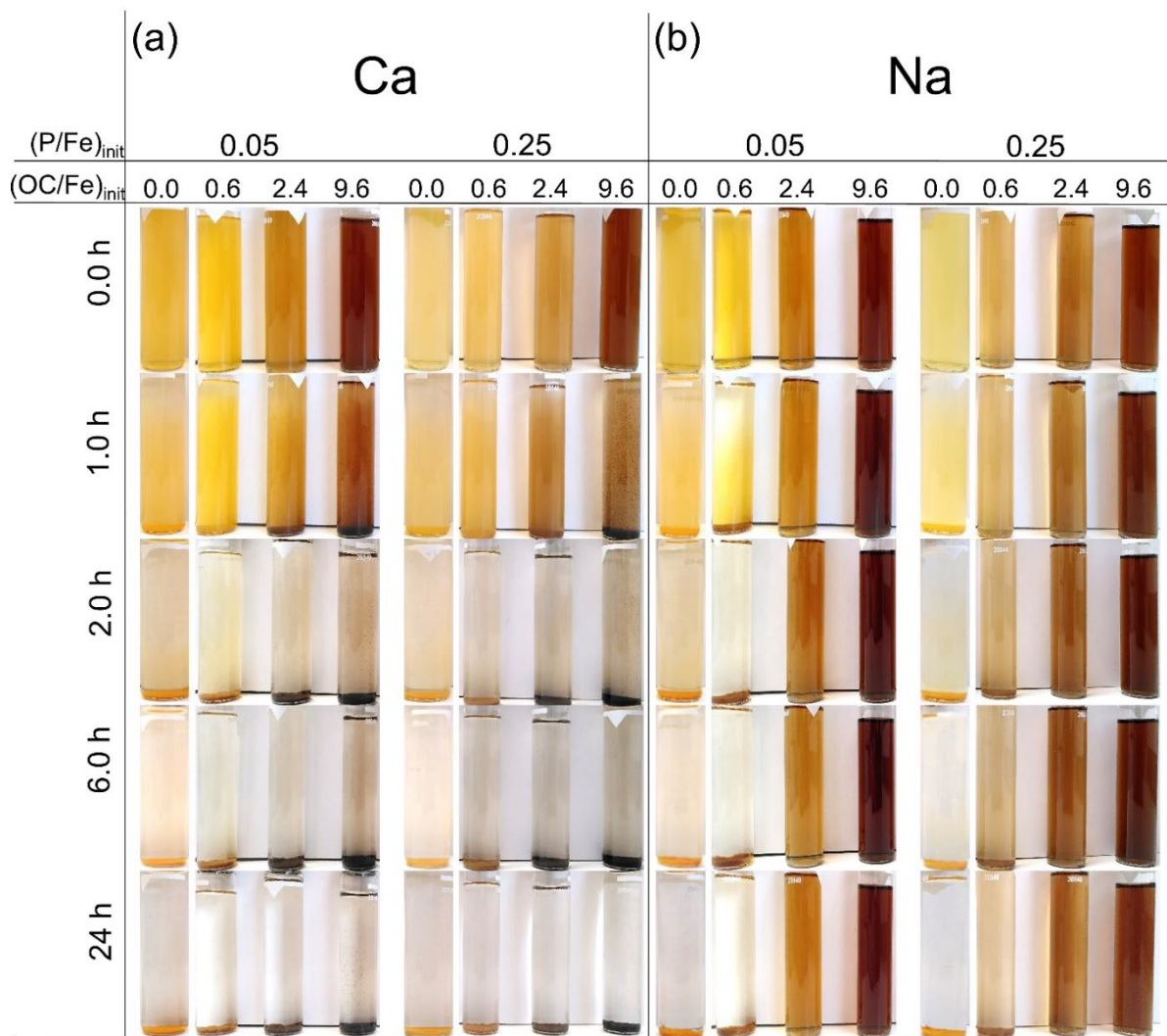


Figure S22. Photos of precipitate suspensions formed in presence of LH; over 24-h settling period upon re-dispersion.

10 TOC analyses in solution

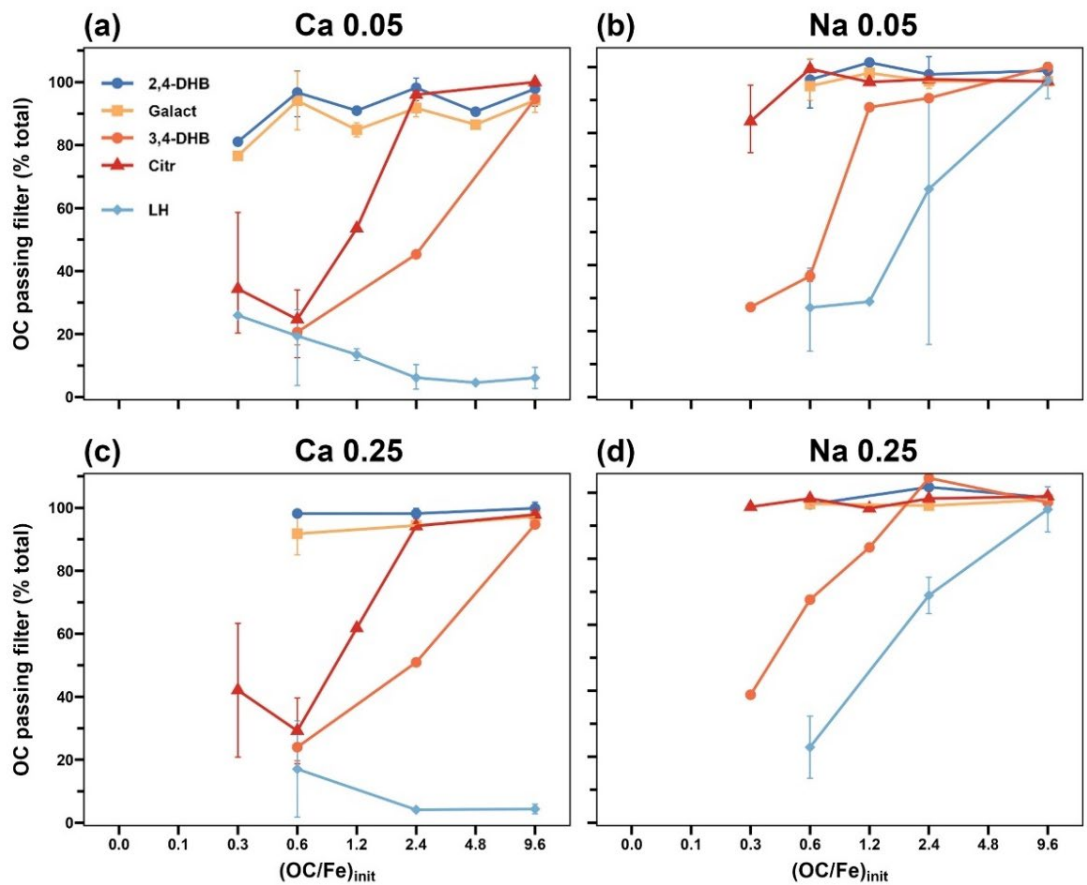


Figure S23. Fractions of total organic carbon passing the 0.2-μm filter membranes (% of total OC in suspension). The averaged blank values (from 3 blanks) of 0.6 mg/L OC was subtracted from all the data for background correction. Points with error bars represent standard deviations from triplicate experiments (where available).

Table S14. Total organic carbon (unfiltered initial solutions and final suspensions) in Na electrolyte solutions with $(\text{P}/\text{Fe})_{\text{init}}$ 0.05 before (initial) and after 18-h oxidation period.

Ligand	$(\text{OC}/\text{Fe})_{\text{init}}$	TOC (mM)	
		Initial	After Fe(II) oxidation
2,4-DHB	2.4	1.33	1.31
	9.6	4.85	4.79
Galact	2.4	1.24	1.23
	9.6	4.81	4.90
3,4-DHB	2.4	1.19	1.18
	9.6	4.75	4.72
Citr	0.3	0.18	0.19
	0.6	0.31	0.30

11 UV-Vis

Completion of Fe(II) oxidation within 18-h reaction period

To validate that Fe(II) oxidation was complete after the 18-h reaction period, selected samples were analyzed for residual total Fe(II) using UV-Vis spectrophotometry. After the reaction period, 5 mL of the unfiltered suspensions containing 0.5 mM total Fe were collected, acidified with 1.0% HCl (v/v), and reacted overnight in the dark to dissolve Fe-precipitates and release organically complexed Fe into solution. Subsequently, the aliquots were spiked with 0.5 mL 0.2% w (~0.11 mM) 1,10-phenanthroline solution, diluted 1:10 with DDI water in a plastic cuvette (polymethylmethacrylate (PMMA); 250 μ L of solution to 2.5 mL water), and analyzed using a UV-Vis spectrophotometer (Cary 1E, Varian). Comparison of the sample spectra with calibration spectra indicated that Fe(II) was below the LOD of 0.6 μ M; i.e., below 6 μ M prior dilution and thus below ~1% of the initial 500 μ M total Fe(II) (Fig. S24).

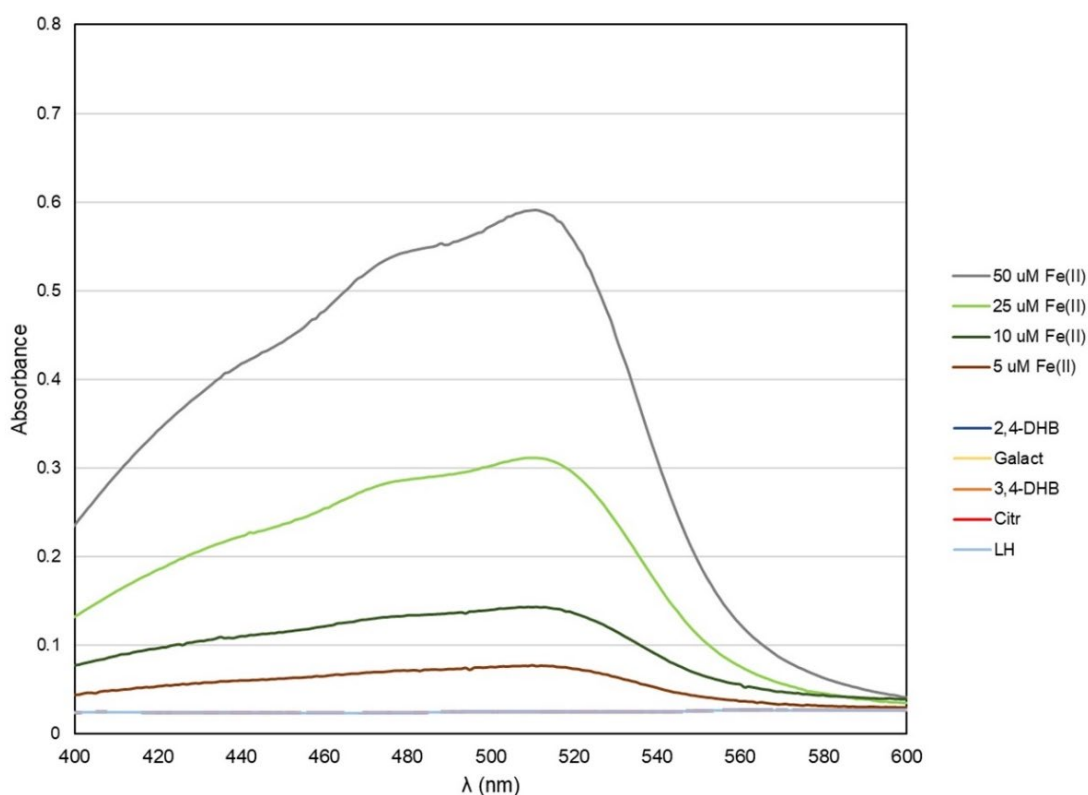


Figure S24. Quantification of residual total Fe(II) in unfiltered precipitate suspensions after acid dissolution using the phenanthroline method. Sample spectra were collected on 10-fold diluted solutions from experiments with 2,4-DHB, Galact, 3,4-DHB, Citr and LH at $(OC/Fe)_{init}$ 9.6 in Ca 0.05 electrolyte.

UV-Vis spectra of filtered 3,4-DHB-Fe(III)-suspensions and of dissolved 3,4-DHB

UV-Vis spectra were measured of 0.2- μm filtered suspensions after Fe(II) oxidation and of dissolved 3,4-DHB at the same concentration. The spectrum of dissolved 3,4-DHB in Fe-free Ca electrolyte shows absorption bands at 250 and 290 nm. In the filtered Fe(III)-precipitate suspension samples, these bands shifted to 234 and 310 nm, and an additional broad band appeared at 560 nm, indicative of Fe(III)-catechol complexation (Fig. S25).⁴ Considering that catechol oxidation to ortho-quinone would have resulted in a strong absorption peak at 390 nm⁵ that was not observed in the filtered suspensions, the UV-Vis spectra indicated that 3,4-DHB was not oxidized to detectable extent.

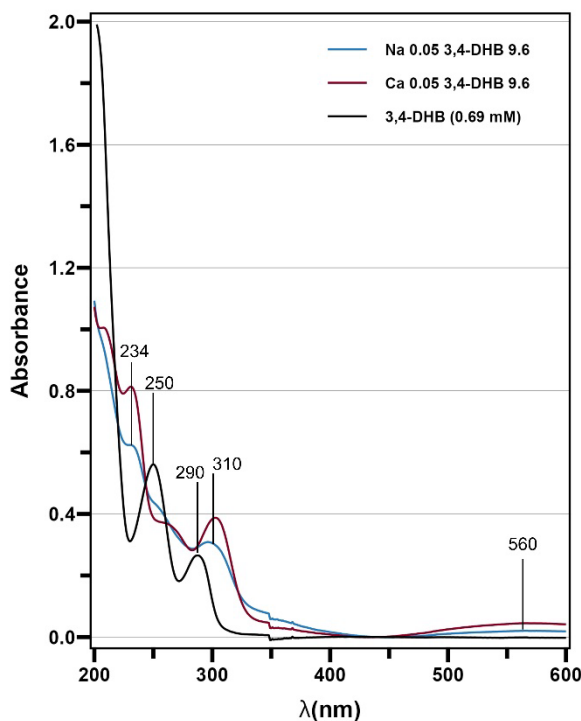


Figure S25. UV-Vis spectra of 0.2- μm filtered Ca 0.05 3,4-DHB 9.6 (red line) and Na 0.05 3,4-DHB 9.6 (blue line) suspensions after the 18-h reaction period in comparison to the spectrum of the same concentration of 3,4-DHB (0.69 mM) in Fe-free Ca-electrolyte at pH 7.0 (black line); over the wavelength ranges 200-600 (nm).

12 Ligand/Fe ratios of selected precipitates and of LCF-based precipitate fractions

Table S15. Calculation of molar ligand (L) over Fe (L/Fe)_{ppt} ratios in bulk precipitate (based on (OC/Fe) _{ppt} from Table S5) and of (L/Fe) ratio in EXAFS-LCF-derived Fh or Fh+FeOrg fractions (assuming that all OC was associated with respective Fe fractions); for selected treatments at (OC/Fe) _{init} 9.6 (2,4-DHB, Galact, 3,4-DHB) or 0.6 (3,4-DHB, Citr). Averaged values of $(L/Fe)_{Fh(FeOrg)}$ are shown for L at both (P/Fe) _{init} and for 2,4-DHB and Galact in all considered treatments.

Electr	(P/Fe) _{init}	Ligand	(OC/Fe) _{init}	(OC/Fe) _{ppt}	(L/Fe) _{ppt}	Fh	$(L/Fe)_{Fh}$	$(L/Fe)_{Fh}$ for (P/Fe) _{init} 0.05 and 0.25	$(L/Fe)_{Fh}$ for L average (SD)
Ca	0.05	2,4-DHB	9.6	0.35	0.05	0.69	0.072	0.067	0.055 (0.013)
Ca	0.25	2,4-DHB	9.6	0.23	0.03	0.53	0.062		
Na	0.05	2,4-DHB	9.6	0.23	0.03	0.67	0.049	0.044	0.090 (0.016)
Na	0.25	2,4-DHB	9.6	0.12	0.02	0.45	0.038		
Ca	0.05	Galact	9.6	0.46	0.08	0.80	0.096	0.100	0.090 (0.016)
Ca	0.25	Galact	9.6	0.45	0.08	0.72	0.104		
Na	0.05	Galact	9.6	0.33	0.06	0.88	0.063	0.081	
Na	0.25	Galact	9.6	0.25	0.04	0.42	0.099		
Electr	(P/Fe) _{init}	Ligand	(OC/Fe) _{init}	(OC/Fe) _{ppt}	(L/Fe) _{ppt}	Fh+FeOrg	$(L/Fe)_{Fh+FeOrg}$	$(L/Fe)_{Fh+FeOrg}$ average	
Ca	0.05	3,4-DHB	9.6	2.65	0.38	0.84	0.451	0.451	
Ca	0.25	3,4-DHB	9.6	1.88	0.27	0.58	0.463		
Ca	0.05	3,4-DHB	0.6	0.57	0.08	0.82	0.099	0.094	
Ca	0.25	3,4-DHB	0.6	0.44	0.07	0.82	0.089		
Ca	0.05	Citr	0.6	0.46	0.08	0.94	0.082	0.077	
Ca	0.25	Citr	0.6	0.36	0.06	0.83	0.072		

13 References

1. D. L. Parkhurst and C. A. J. Appelo., User's Guide to PHREEQC (Version 2): A Computer Program for Speciation, Batch-Reaction, One-Dimensional Transport, and Inverse Geochemical Calculations., *U.S. Geological Survey, Denver, CO.*, 1999.
2. R. Smith, A. Martell and R. Motekaitis, NIST Critically Selected Stability Constants of Metal Complexes., *NIST Standard Reference Database 46, Version 8.0.*, 2004.
3. S. Deiana, C. Gessa, V. Solinas, P. Piu and R. Seeber, Analytical study of the interactions of D-galacturonic acid with iron(III) and iron(II) in solution and with iron(III)-bentonite, *Anal. Chim. Acta*, 1989, **222**, 315-322.
4. M. Elhabiri, C. Carrér, F. Marmolle and H. Traboulsi, Complexation of iron(III) by catecholate-type polyphenols, *Inorg. Chim. Acta*, 2007, **360**, 353-359.
5. G. Albarran, W. Boggess, V. Rassolov and R. H. Schuler, Absorption spectrum, mass spectrometric properties, and electronic structure of 1,2-benzoquinone, *J. Phys. Chem. A*, 2010, **114**, 7470-7478.